UNIVERSITY OF BIRMINGHAM

School of Metallurgy and Materials

Master by Research (MRes) Dissertation

Direct Laser Fabrication of Ti-5553

Submitted by:

Arash Hatefi

Supervisor:

Dr. Moataz M.Attallah

ACKNOWLEDGEMENTS:

I would like to express my gratitude and love to my family for their continuous support and never ending understanding during my study.

Great appreciation goes to my supervisor Dr. M. M. Attallah and also Dr. Ravi Aswathanarayana Swamy and for his unconditional help and support. I always appreciate their support during this part time study, taking into notice my situation with full-time employment and the support provided to me during this time.

I would also like to express my gratitude towards the School of Metallurgy and Materials at the University of Birmingham for offering me the opportunity to study part time.

Great appreciations towards my colleagues at Messier-Bugatti-Dowty Reasearch & Development department, Mr. Simon Harris & Garmain Forgeoux and Przemyslaw Grochola. Special thanks to my department manager Mr. Colin Jones, MBD Supplier Quality Manager, for giving me the chance and the opportunity for pursuing my study, despite the busy work schedule in the department.

ABSTRACT

Titanium alloy Ti-5553 PREP® powder has been processed using Direct Laser Fabrication (DLF) technology to assess the feasibility of using DLF to produce certain features on existing aerospace structures, in a hybrid additive layer manufacture (ALM) approach. A range of laser processing conditions has been utilised in order to understand the influence of those conditions on the mechanical properties and microstructure of the DLFed samples.

The experiments showed that processing parameters have significant effect on the properties of the DLFed samples. Those effects were not just limited to the physical properties but also affect the metallurgical properties of the samples. Grain sizes found to increase in size as the build progresses. The micro-section of the interface and the deposition layers did not show any sign of porosity.

Within the present work, Optical microscopy and Scanning Electron Microscopy (SEM) were used to assess the microstructure of the DLF produced samples.

Heat treatment cycles have been reviewed to establish the most effective method for improving the properties of as-DLFed samples to achieve the desired properties. Ageing cycles as well as Solution treat + Ageing cycles have been considered and the mechanical properties tested for samples in each condition.

The microstructures showed that as-DLFed samples did not contain the α-precipitates necessary to achieve the desired mechanical properties. Ageing cycle can slightly improve those properties but only through the solution treatment and aging cycle, the desirable mechanical properties can be achieved. Once the samples are Solution treated and aged, significant volume of primary α-phase would precipitate within the aged β-matrix.

ACKNOWLEDGMENTS

Table of contents

Introduction

Landing gears are major part of all aircrafts flying around the world. Safely taking off and landing of the commercial aircrafts as well and military planes are dependent on the safe and correct deployment of those aircrafts landing gears. The need for improved and cost-effective processes as well as smarter material utilisation has led to recent developments and advances in near net-shape technology and processes.

This project has been established and undertaken in order to evaluate the practicality of using direct laser fabrication (DLF) technology, to produce features such as holding lugs on landing gear parts using Ti-5553 alloy. The main objective in this project is to establish if the DLF process can be utilised to produce such features on the blank forged pats, instead of complicated forging dies with excess material that need to be partially or completely removed during the follow up machining processes.

The research project will focus on the fabrication of lugs on “Truck Beam” for a major aircraft manufacturer main landing gear. At present, truck beam is produced from forging blanks and the lugs are an integrated part of the forging. Figures 1 and 2 show the graphic representations of the truck beam, in the as-forged condition and following the completion of all machining operations.

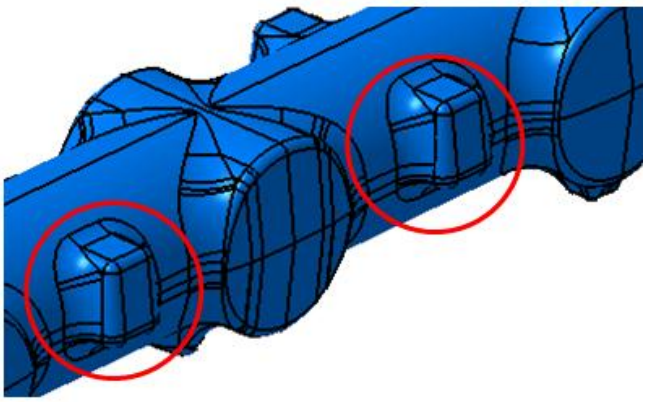

Figure 1: Part of the landing gear truck beam in the as-forged condition. The lugs are produced at the forging stage. Picture courtesy of MBD Gloucester Ltd.

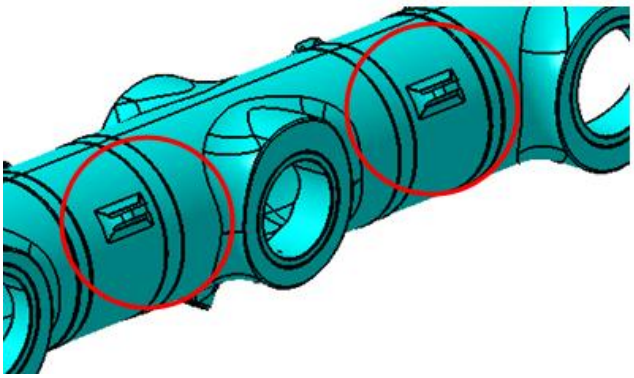

Figure 2: The same part as figure 1 after machining operations. Picture courtesy of MBD Gloucester Ltd.

Further information about the design and manufacture of the truck beam are described in Appendix B.

Section 1 of this report provides an introduction into titanium and its alloys, in particular Ti-5553 which is the subject of this investigation. The literature review section explains the researches carried out in the Direct Laser Fabrication method as well as metallurgy of Ti-5553.

Section 2 explains the experimental procedures used during this study. The section discusses the material, preparation and composition, Ti-5553 powder used for the deposition process, process parameters setup for DLF process, the experimental program and the number of samples, fabrication stages, microscopically evaluation methods and mechanical test procedures.

Section 3 explains the variation within processing parameters which were reviewed and modified to obtain the desired fabricated samples. The section also describes the experimental procedures for the initial deposition and fabrication of the Ti-553 samples and the metallurgical and mechanical tests carried out. The improvements within the microstructure achieved through heat treatment cycles on the fabricated samples will also be described in this section.

Section 3 also presents and discusses the results obtained from the experimentation. Those results include the initial microstructure, hardness test

results and mechanical test results in comparison with Ti-553 in forged condition. The results following the rectification processes will also be discussed in this section.

It must be noted the concept of the Design of an Experiment was discussed and considered in section 3; however the number of test samples that were produced satisfactorily as the result of variations of the processing parameters did not produce adequate information to investigate correlations between the processing parameters and the volume of the porosity within the micro-section.

Section 4 summarises the results and presents the conclusions from the thesis, explaining the effects of processing parameters and rectification processes to improve the microstructure of deposited Ti-5553. This section also suggests future work to be carried out to further investigate the DLF parameters and the effects of those parameters on the material properties.

1 Literature Review

1.1 Introduction to Titanium

Titanium and its alloys are relatively new to the field of structural materials compared with steel and aluminium alloys. Discovered in 1790 by W. George and M.H. Klaproth [1], the interest in using Titanium as a structural material began to develop in 1940's and 1950's. This interest was the result of high specific strength, excellent corrosion resistance and fracture toughness compared to traditional metals such as steels and stainless steels.

The following section will give an overview on the titanium alloy classes, and their respective properties.

1.2 Titanium and its alloys

Various industries use a wide range of pure and alloyed titanium in various product forms such as mill products, castings, forgings and powder metallurgy product. However not each alloy or grades of titanium is available in all forms and sizes of products. In many cases, alloying elements are added to pure titanium to improve certain properties of the material. The following sections briefly explain the roles of alloying elements in developing titanium alloys.

When alloying elements are added to Commercially Pure Titanium (CP Ti), Titanium develops a number of features that separate this material from the other light metals and make its physical metallurgy both complex and interesting. A summary of those features is listed here:

At 882˚C pure Ti goes through an allotropic phase transformation from a Hexagonal Close Packed (hcp) microstructure to the Body Centred Cubic (bcc) or beta (β) phase that stays stable up to the melting point. It is the result of this

transformation and similar to steels, various heat treatment processes would develop α, β or mixed α/β microstructure alloys. [2]

Titanium is considered as a transition metal containing an incomplete shell in its electronic structure that enables this material to form solid solutions microstructures with most alloying elements having a size factor within ±15%. [3]

1.2.1 Alloying Elements

Both mechanical and physical properties of titanium are greatly affected by adding alloying elements to it. Each alloying element that can be added to titanium in either small or large amounts, would change the basic crystal structure of the material that in turn would affect the strength of the material.

Apart from the change in the strength of titanium, the change in the crystal structure transformation is another major effect of addition of alloying elements to titanium. The transformation that happens at about 882ºC in CP-Ti. This effect is in the form of increase or decrease on the transformation temperature and depends on the type of the added alloying element. Based on the effect of the alloying elements on the distortion of the crystal structure, this effect can be stabilisation of either α or β phases at lower temperatures.

Titanium alloy phase diagrams are often complex and are not readily available. However in general 3 categories of titanium alloys are developed through addition of alloying elements, as shown in figure 1-1: α and near α alloys, α+β alloys and β alloys.

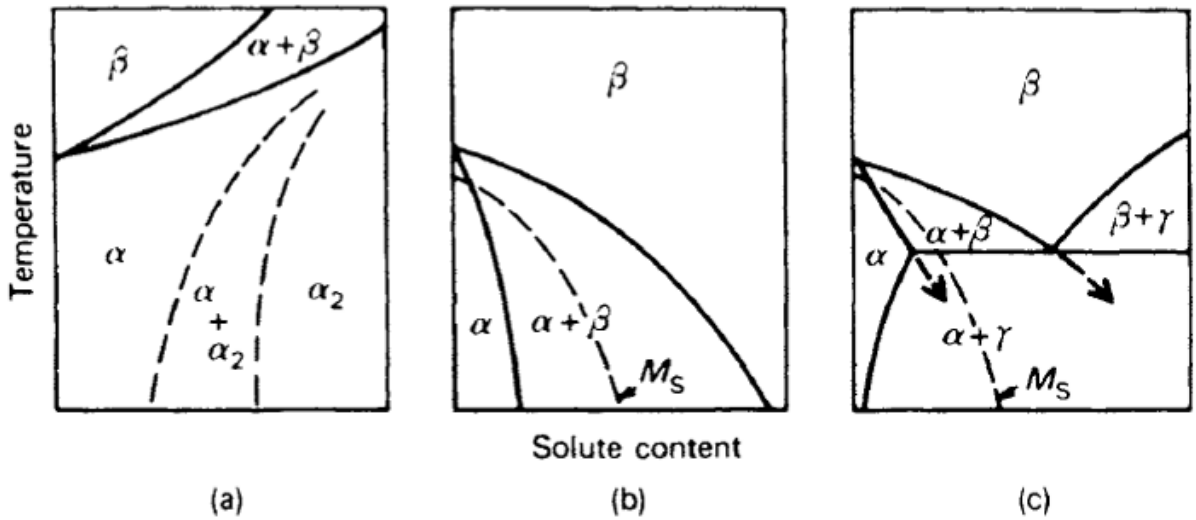

Figure1-1: Basic types of phase diagrams for titanium alloys. The dotted phase boundaries in (a) refer specifically to the Ti-Al system. The dotted lines in (b) and (c) show the Martensite start (Ms) temperatures. Alloying elements favouring the different types of phase diagrams are (a) Al, O, N, C, Ga; (b) Mo, W, V, Ta; (c) Cu, Mn, Cr, Fe, Ni, Co, H. [1]

- **α and near α alloys:**

α-alloys are the result of addition of alloying elements that stabilise the α-phase such as Fe or V. The mechanism of the stabilisation is by the increase in the α/β transus temperature. The microstructure of α-alloys mainly consists of α phase with the small amount of β phase precipitated at α grain boundaries [4]. α-alloys do not show good weld-ability because of a lack of response to heat treatment and are good for sub-zero applications as they do not have a ductile-to-brittle transition. Forge-ability of the alloys is not good as the result of the "hcp" structure of α phase. α-alloys have excellent corrosion resistance properties since the oxide layer is very stable.

- **α/β alloys:**

The α/β titanium alloys are the mostly used titanium alloys for commercial applications. This category of titanium alloys accounted for more than half of all titanium usage in the U.S. in 1998 with 56% of the total usage being Ti-6Al-4V

[4]. In comparison to near α-alloys, a small but considerable volume fraction of β-phase is still present at room temperature as the result of the presence of α and β stabilizing elements. An attractive balance of characteristics including a positive combination of strength, ductility, fatigue and fracture properties is developed within this group of alloys due to the combination of the characteristics of each phase. The microstructure can be changed by modification of the solution and aging temperatures and times and also cooling rates from above the β transus. [4]

α/β titanium microstructures are formed by addition of alloying elements which depress the α/β transus and increase β-phase stability. Those alloying elements may be classified in two categories: a) those elements that develop binary systems of the β-isomorphous [5] type (figure 1-1(b)) and the group of element that increase chance for formation of a β-eutectoid (figure 1-1(c)).

- **Metastable β alloys:**

Titanium alloys containing adequate quantities of β-stabilisers to hold back the Martensitic transformation and subsequently retaining the bcc crystal structure on quenching to room temperature are classified as Metastable β-titanium alloys. [6]

A large volume fraction (~ 40%) of β-phase is retained within the β-metastable titanium alloys at room temperature after heat treatment. The microstructure contains initial β-grains and the α-phase precipitating with various morphologies: needles, nodules, etc. This group of alloys have high tensile and fatigue strength but poor elevated temperature creep and oxidation resistance. [6]

Addition of β-stabiliser elements to the alloy would result in the reduction of the beta transus temperature down to below room temperature and subsequently a stable β-Ti alloy [7]. Metastable β-Ti alloys exhibit good formability [8] and although it is well known that beta titanium alloys do not work harden

significantly, a significant rate of work hardening has been reported by *J. Ph. Guibert & et al.* for Ti–20V under compressive testing [9]. However the deformation and work hardening properties of various titanium alloys are not covered as part of this study.

Metastable β-Ti alloys are typically subject to a thermo-mechanical treatment to precipitate additional phases. Through solution treating and precipitation of α, ω phase and/or intermetallic yield strength and fracture toughness of these alloys can be improved. The morphology, size and distribution, of these precipitates greatly affect the mechanical properties of the alloy. [7]

Metastable β alloys do not form martensite but retain the β phase after quenching to room temperature. As the result of high hydrogen tolerance of the β-phase, the corrosion resistance of metastable alloys is good and in some aspects even better than α/β alloys. Due to slow α-phase kinetics, thick sections of these alloys can be heat treated to produce a constant microstructure. [7]

1.2.2 Ti-5553 development

Near β titanium alloys, that can be quenched to room temperature whilst still retaining a fully β phase microstructure, are candidates for use in many demanding structural applications where light weight and high-strength are required.

A recently-introduced alloy Ti–5Al–5Mo–5V–3Cr (Ti-5553) (based on Russian patented alloy VT 22 Ti-5.7Al-5.1V-4.8Mo-1Cr-1Fe) is a near β titanium alloy developed for a number of thick-section aerospace components due to its high strength and deep hardenability [11, 12]. The addition of Fe to these alloys has improved the sintering properties of the material for powder metallurgy applications [12].

Titanium Ti-5553 (Ti-5Al-5Mo-5V-3Cr) also known as Timetal, is a metastable β titanium alloy that as previously mentioned has been developed from Ti-5.7Al-5.1V-4.8Mo-1Cr-1Fe. As reported by B.A. Welk in his research report [14] Ti-5553 alloy was initially introduced for aircraft industry in form of large size forgings due to the higher strength of this alloy compared to VT22 as well as reasonable ductility. A combination of strength, ductility and toughness improvements has made this alloy significantly more attractive for such forging applications.

S.L. Nyakana, et al. [15] explain that as the result of slow diffusion kinetics of Mo and Cr, the produced α-phase dispersion is refined and subsequent strengths as high as 1517 MPa can be achieved although with limited ductility.

The high hardenability of this alloy allows sections up to 6" thick to be heat treated and air cooled with an insignificant reduction in strength when compared to Ti-10V-2Fe-3Al which has a thickness limit of 3" and must be water cooled [16]. This hardenability and relative ease of production are responsible for Ti5553 replacing Ti-10V-2Fe-3Al used on previous designs of landing gears [17]. Once the material is solution treated above its beta transus temperature, then a lamellar or bi-lamellar (secondary α) microstructure can be produced. Solution treatment below its β transus temperature would develop a bimodal microstructure.

As mentioned above, Ti-5553 alloy is used for parts such as large landing-gear forgings and high-strength fasteners in the new generation of commercial airliners [17]. As described by G.Lutjering [18] the slow precipitation kinetics of α-phase compared to other β titanium alloys such as Ti-10-2-3 makes Ti-5553 alloy a good candidate for thick section forgings for high strength airframe components such as landing gears or flap tracks.

Considering the recent developments on Ti5553 alloy, few technical papers are currently available investigating mechanical and various properties of this alloy under different conditions. However J.C.Fanning [19] study of Ti-5553 (referred to as TIMETAL) suggests that the alloy in solution treat and aged condition could achieve the following mechanical properties:

Tensile mechanical properties					
Ultimate, ksi (MPa)	Yield @ 0.2%, ksi (MPa)	El (4D), %	RA %	Compression yield @ 0.2%, ksi (MPa)	Shear ultimate, ksi (MPa)
179.2 (1236)	170.3 (1174)	13	25.4	…	…
…	…	…	…	170.1 (1173)	…
…	…	…	…	…	99.5 (686)

Table 1: Average longitudinal mechanical properties of TIMETAL 5553, 22 mm (0.87 in.) bar in solution heat treated plus aged condition as studied by J.C.Finning [19]

Further studies have been carried out on the influence of alloying elements on precipitation of α-phase in Ti-5553. Study on the influence of carbon on such precipitation [20] concludes that carbon affects the precipitation of isothermal 'ω' at low ageing temperatures, but not at higher temperatures. Also the precipitation of α phase during ageing stage is not strongly affected either by the presence of carbon or by low-temperature ageing when the material is quenched from below the β transus.

The study also suggests that the balance of mechanical properties in Ti-5553 is expected to be dependent on the volume fraction, size, morphology and distribution of α-precipitates within the β-matrix. By varying the heat treatments parameters such as temperatures, times and cooling rates, various volume fractions and morphologies of α-phase nucleated within the β-matrix phase can be achieved in this alloy. The partitioning of the alloying elements, Al, V, Mo, Cr and Fe, also depends on the applied heat-treatments. Furthermore, in addition to these primary alloying elements, interstitials such as oxygen and hydrogen can also play a significant role on the development of the microstructure in this alloy. The nucleation sites for α-phase within the β phase of this alloy include prior β

grain boundaries, β/ω interfaces, β/β' interfaces and other defects such as dislocations and intermetallic particles within the matrix [21].

Figure 1-2 shows the microstructure of the Ti5553 using SEM microscope. The β-phase is white and the α-phase is dark.

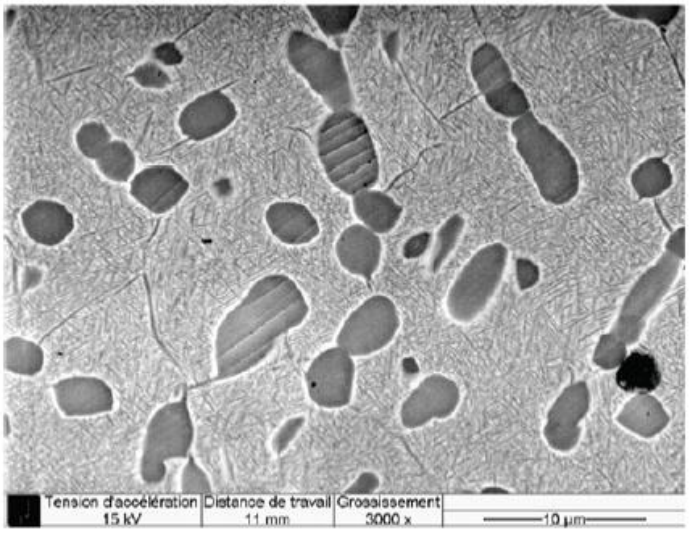

Figure 1-2: SEM BSE image of Ti5553 microstructure showing β-phase in white and the α-phase in dark contrast. [17]

1.3 Heat treatment of Ti 5553

The response of Ti5553 to heat treatment has been subject to a number of studies. Shevel'kov [22] performed his work on study of the phase transitions in VT-22 upon water quenching to room temperature from 950°C. Using x-ray analysis, the study showed that there was β-decomposition upon quenching. The study also suggests that α" appearance has occurred by a shear mechanism in the β solid solution starving regions. Nucleation of α from the β starving regions was seen to occur at 500°C after only 0.1h.

A.Dehghan & R.Dippenar studied [13] the isothermal heat treatment of Ti-5553 and concluded ageing time and temperature have direct impact on the volume fraction of α-phase precipitated from the β-matrix. The study suggests that by increasing the aging temperature from 625K to 725, the volume fraction of precipitated α-phase was increased by 6 times from 5% to 30%. The ageing

temperature also changes the morphology and size of precipitated α. The study was carried out from solution treatment and only considers the effect of ageing cycles.

B.A. Welk's study [14] previously discussed also refers to the study of heat treatment of Ti-5553 carried out by Orlova [23] for the changes in microstructure caused by varying the T1 (solution) temperature and the T3 (aging) temperature of an industry standard heat treatment . B.A. Welk explains that the study mentioned herein has concluded that the rate of the grain growth is significantly higher at Solution temperatures (T1) which results in lowering the strength and the ductility of the samples. At that temperature the β-matrix also changes and coarse α-laths stat appearing along the grain boundaries. On the other hand, reducing the T1 temperature will cause an increase in the spreading of the secondary α-phase alongside a reduction in the precipitation of the tertiary α-phase.

Material specification MTL 3103 [24] has been specifically developed by Messier-Dowty Ltd describing the requirements for Titanium Ti-5553 alloy and the responsibilities of raw material and forging producers in the production of ingot, bars and forging stocks for subsequent heat treatment to a tensile strength of at least 1240 MPa at ruling sections up to and including 150 mm. However due to the confidentiality of the material specification, only the essential requirements of this material as applicable to this study have been described herein. The microstructure requirements of MTL 3103 [24] after the heat treatment, are that the microstructure shall consist of a primary alpha phase in an aged beta matrix. A continuous alpha phase network along beta grain boundaries is undesirable, but need not be a reason for rejection if the tensile and K_1C characteristics are satisfactory. The reference heat treatment requirements as specified by MTL 3103 are:

(1) Solution heat treatment: soak for 2 hours at a temperature of (βT – 40 °C ±10 °C) (βT – 72 °F ±18 °F).

(2) Air cool

(3) Ageing treatment: soak for 8 hours at 610°C ±5 °C (1112 ±9 °F)

(4) Air cool

Following the above reference heat treatment, the mechanical properties of the material shall meet the requirements of table 2:

Direction	**0.2% Proof Stress MPa**	**Tensile Strength MPa**	**Elongation %**
	Min	**Min Target Max**	**Min**
Longitudinal	1170 (170)	1240 1290 1410 (180) (186) (205)	6
Transverse	1170 (170)	1240 1290 1410 (180) (186) (205)	4

Table 2: Mechanical properties requirements from Messier-Dowty MTL 3103 [36]. Vales in ( ) are in KSI

1.4 Laser Fabrication technology

Direct Laser Fabrication, also known as Directed Metal Deposition, Laser Powder Deposition, Laser Direct Manufacturing and Electron Beam Free Form Fabrication, is a rather recent development that can potentially help to reduce the cost of manufactured parts. A focused laser beam is used to melt powder and deposit the melt in a predetermined path on a substrate as shown in figure 1-3.

The metal deposited perform is then machined to the final part shape. Such near net-shape manufacturing method once adequately developed and optimised, could lead into saving in materials, machining costs and cycle times over conventional forged or machined parts. [25]

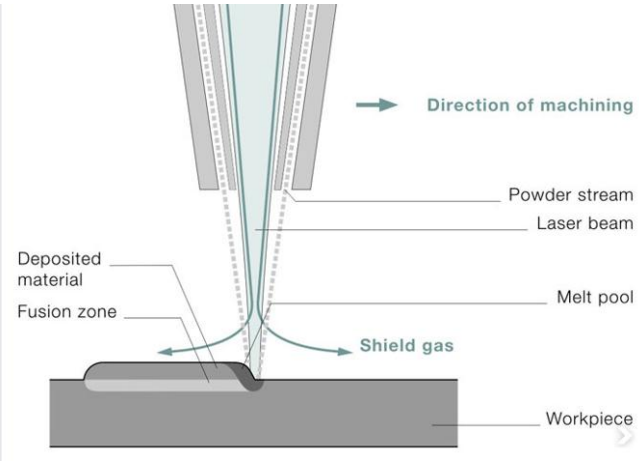

Figure 1-3: Typical application of DLF. The laser is used to generate a molten bath on the prepared surface. Powdered material is guided through the nozzle, step by step. Once the new material has cooled, the next layer is deposited , or the refinishing process starts. Image courtesy of Trumpf Groppe.

Direct laser fabrication (DLF) is a technology that utilises the basis of laser cladding to create 3-D metallic structure by layer by layer deposition of molten material. Today, 2 main types of laser fabrication technologies are being used: Powder bed and Direct Laser Fabrication (DLF). Although it must be noted that the Powder laser bed technology was initially developed for rapid prototyping and later on it has been developed for the production of engineering components. In this technology, successive layers of powder are spread uniformly across the bed and a laser follows a path defined by a CAD program to produce a 2-D slice of the component. The bed is then lowered and the next layer of powder is spread over the previous layer. The increment in the height of the component is developed by this downward movement of the bed. The unused powder on the powder bed is loose and can be completely recycled.

Similarly the DLF technology also utilises focusing of a high power laser onto to a small focal point, typically 1-2mm in diameter whilst the metallic powder is also blown into this focal point. At this spot, the high power densities of laser induce large thermal gradients resulting in the formation of a melt pool. Metal powders are delivered at the focal spot either through gravity or by the pressure of an inert gas. The inert gas also creates a shield around the molten pool to reduce the risk of oxidisation. Through movement of the table in both X and Y directions, layer by layer deposition is carried out on a substrate. Figure 1-4 [26] shows a schematic setup of the DLF process.

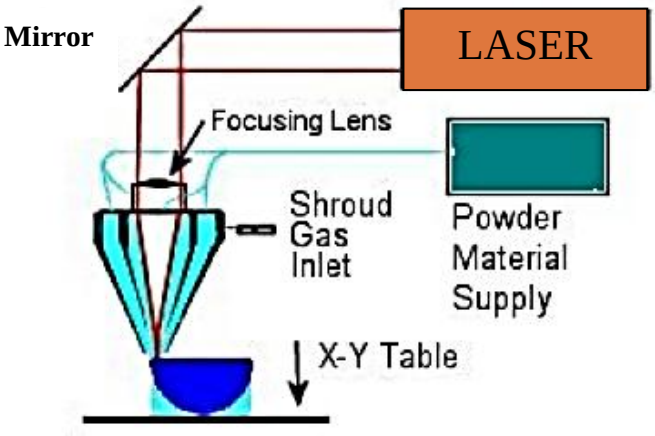

Figure 1-4: Schematic diagram of DLF process. The main elements of the process include: The laser source, the focal point size, the powder, and the carrying gas. [26]

The size of powder used in the powder bed technology is less than 20µm compared to the typical powder sizes used in the direct feed technology which tend to be around 90 – 120µm. As the result, the surface finish of powder bed products is far smoother than in typical DLF components, however this improvement is achieved by compromising the cost of very small Z increments, hence the prolonged build-time.

In DLF technology, the powder is fed at a controlled rate into the focal point of the laser where it is melted into the melt pool, as the movement of the laser follows the path defined by a CAD (computer aided design) file of a component;

this CAD file controls the movement of the sample in the X–Y plane and the movement of the laser along the Z axis.

This technology is particularly well suited to the repair of components and is currently being applied to the repair of compressor and turbine blades and of tooling. A study on the net shaping manufacturing of Aeroengine Components using DLF technology [27] used a 3-D finite element model to simulate the thermal profile of a Ti 6-4 sample during the fabrication stage using DLF technology. The results showed a good match between the predicted and measured thermal profiles. The thermal profiles at various locations on the fabricated parts were also consistent with the microstructures obtained.

1.5 Comparison of DLF with Conventional Processing Technologies

DLF is a direct metal deposition process that delivers metal powders into the focal point of a high power laser beam, melts the powder and creates a fully-dense metal deposit. Direct metal deposition can be equipped with computer-based design and numerical control to form 3D near-net shaped parts. It can be a waste-free or waste-minimised process, because it is performed in a high purity inert gas environment in which powder that is not melted by the laser, can be recycled and may be used again. This feature makes the process particularly attractive for expensive, high-performance materials or hazardous materials that require containment during processing. In addition, since the one-step process deposition process produces near-net shape components, further cost savings through reduction or avoidance of further conventional machining, forming operations or powder metallurgy operations are also possible. In addition, higher purity materials can be provided with the elimination of contamination pick-up from cutting tools, dies and forming surfaces, lubricants or cleaning agents. Cost savings can also be achieved through reductions in handling and storage costs, as there are no intermediate processing steps.

1.5.1 Feeding methods

Laser fabricated structures can be produced using Powder or Wire for deposition. Recent studies have been carried out on the differences between the deposition microstructure of these two methods of deposition. *W.U. Syed et al.* [28] studied the DLF process using wire and powder feeding method on steel family of material; however the concept of wire feeding and powder feeding systems can be expanded to Titanium. Figure 1-5a shows the typical setup of the wire feeding system. The study investigated the effects of feeding direction and location and concludes that the best feeding direction for the wire was from the front, compared to the results when the wire was fed from the rear as shown in figure 1-5b.

The results obtained for powder feeding showed noticeable differences compared to wire feeding system. High catchment efficiency was observed when the powder was fed from the front; an increase of 20–45% in efficiency compared to the rear powder feeding for the same operating conditions was reported by the study. However, rear powder feeding resulted in less oxidation and a 20% decrease in the surface roughness.

Nonetheless the study concluded that no noticeable difference could be noticed between the microstructure of the Powder and wire fed system. The micro-structures of both methods were reported mainly as dendritic and cellular with a cell size between 2 and 15 μm. The study also reported that a finer structure was found in the first layer near to the substrate and then the grain size became coarser on moving up the sample. The top layer showed a mainly dendritic structure and these structures was also seen to prevail at layer boundaries.

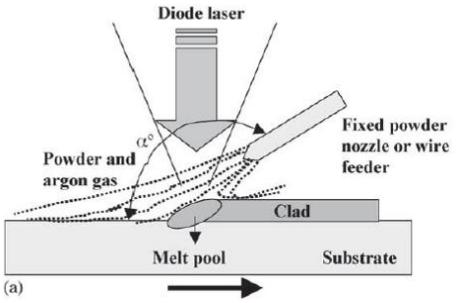

Fig 1-5a: The typical setup of wire feeding system for laser deposition on base metal. [28]

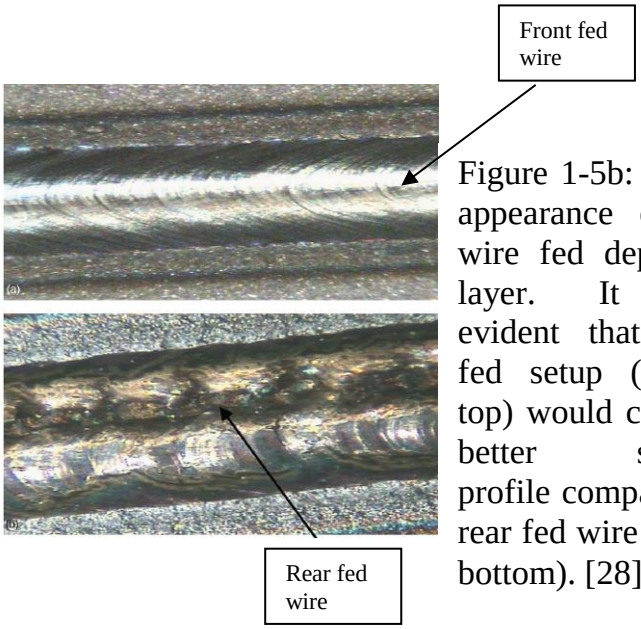

Figure 1-5b: Visual appearance of the wire fed deposited layer. It was evident that front fed setup (at the top) would create a better surface profile compared to rear fed wire (at the bottom). [28]

The SEM results on both wire fed and powder system shows a difference in the pores within the structures. The analysis showed that although no crack existed within the microstructure, porosity was evidence within the cellular and dendritic structure of powder fed samples as shown in figures 1-6 (a) & (b).

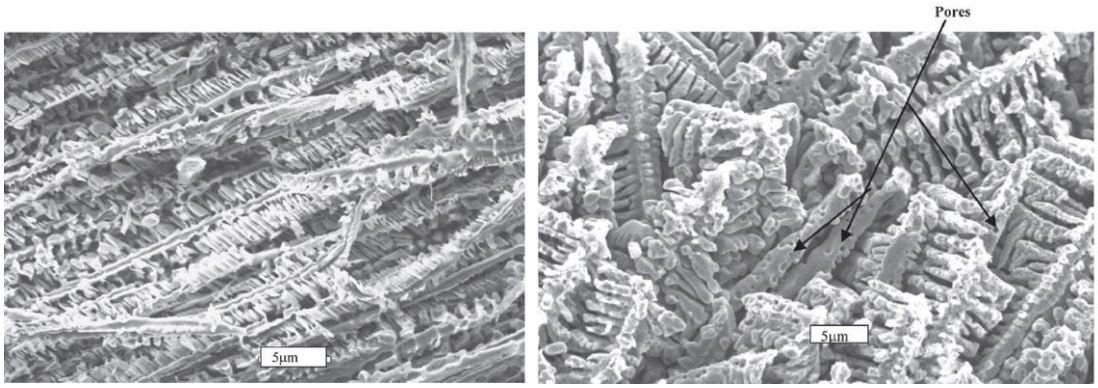

(a)– Powder deposit layers (b) – Wire fed deposit layers

Figure 1-6: (a) Pores as shown on the SEM. The structure compared to the wire fed structure in (b), appear to contain more pores. [28]

The study also showed that a variation of microstructures exist through the thickness of the layers. A finer structure existed in the first layer near to the substrate and then the grain sizes became coarser on moving up the sample. The top layer was reported as dendritic structure.

Other studies [29] on the DLF process has been carried out for the purpose of comparison between 2 different titanium alloys: Ti-6Al-4V and a burn resistant titanium alloy Ti-25V-15Cr-2Al-0.2C known as "BurTi". In the study, Special modifications had been carried out on the powder nozzle in order to ensure the powder feed rate can be adequately controlled. Microstructure analysis of the deposited sample made of wire fed reported to be dominated by columnar grains as shown in figure 1-7a. The study suggests that during laser fabrication, Ti6-4 tends to grow on the previous layer; whereas in laser fabricated BurTi as described in other literatures [30], nucleation normally takes place in every layer of the deposition. The study also suggests that small amount of BurTi would change the microstructure of Ti6-4 from epitaxial growth and subsequently columnar structure as shown in figure 1-7a to nucleation dominating in the deposition so that equiaxed grains form as shown in figure 1-7b.

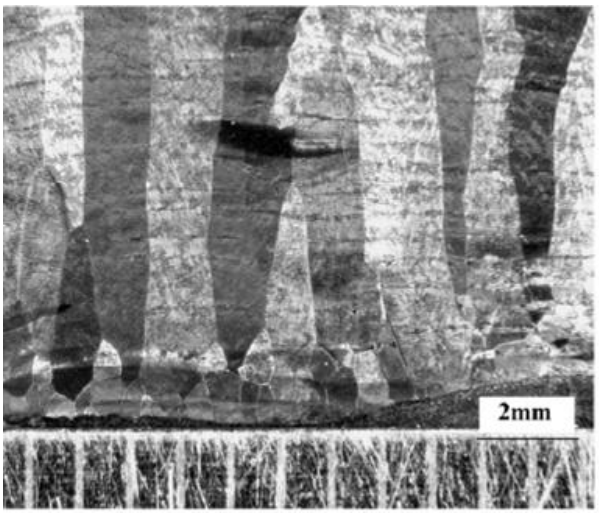

Figure 1-7a: Epitaxial & Columnar growth of the Ti6-4 [29]

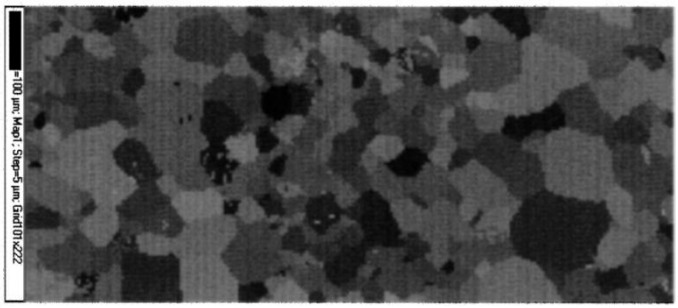

Figure 1-7b: EBSD map showing the equiaxed microstructure which is present in most of a build and much smaller equiaxed grains between the successive layers. [30]

Despite the obvious advantages of the wire fed system, it was deemed impractical to use this system for the purpose of this project since the main focus of this

project is on Ti-5553 alloys. At the present study, only powder form of this material can be produced.

1.6 Process parameters

One of the most important processing parameters affecting the microstructure of all metals is the cooling rate from the melt temperature. The laser power used for the wire-fed system has been reported up to 3 times higher than the power used for the powder fed system. Therefore the temperature of the melt pool in the wire-fed system would be significantly higher that the powder fed system. This higher temperature would result in a significantly reduced cooling rate compared with the powder fed system. As a result of this higher heat input, the micro-structure of the wire-fed samples was reported as Widmanstatten as shown in figure 1-8 rather than Martensite as observed when using powder.

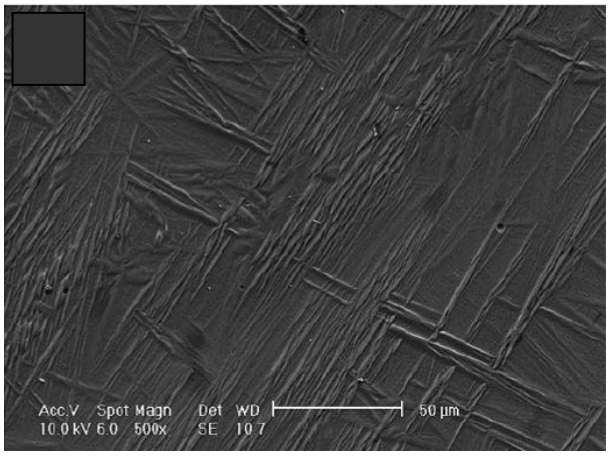

Figure 1-8: SEM image of the Widmanstatten structure of wire fed samples. [29]

X.Wu & *et al*. [31] study of the processing parameters on DLF identified 4 major processing parameters for the DLF process. These parameters are: **Laser Power**, **Powder Feed Rate**, **Laser scanning rate** and **the Z increments**.

The study was undertaken using Ti6-4 powder and collection of parts were manufactured. The study showed that using Ti6-4, the two sides of a single layer pass wall tend to solidify faster than the middle of the wall, which tends to create a hollow wall. The study also showed that the laser power and the Z increment

have greater effect on the microstructure of the fabricated part. A medium laser power of 245W had produced a nearly 100% dense structure whereas the higher power of 390W some pores were reported at the primary β grain boundaries. Lower laser powers of 180W developed porous structure with connected pores up to 300μm diameter. This experiment was carried out using a feed rate of 6 g/min, scan speed of 200 mm/min and a Z increment of 0.3 mm/min.

The laser scanning speed also has a significant impact on the properties and the microstructure of the deposited layers. The study also concluded that within a range of the scanning speeds, increasing the speed would lead to a finer microstructure up to a point but the microstructure becomes coarser at the extreme speed of 1000 mm/min. It must be noted that the powder feed rate was also increased from 6 to 18 g/min in order to compensate for the higher speed rates. A summary of the results obtained within the study is shown below (figures 1-9a to 1-9c & 1-10a to 1-10c) with representative images.

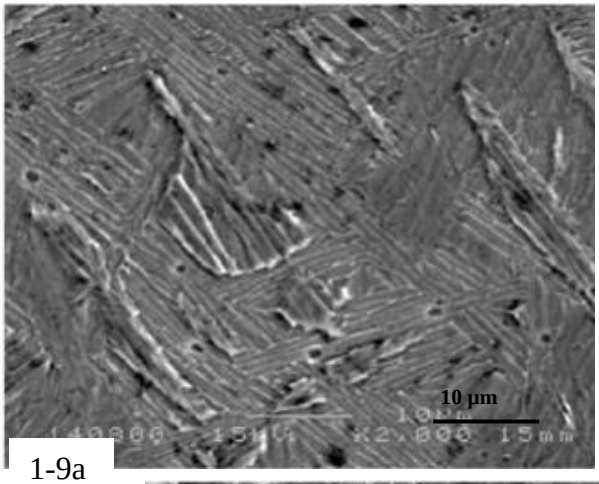

1-9a

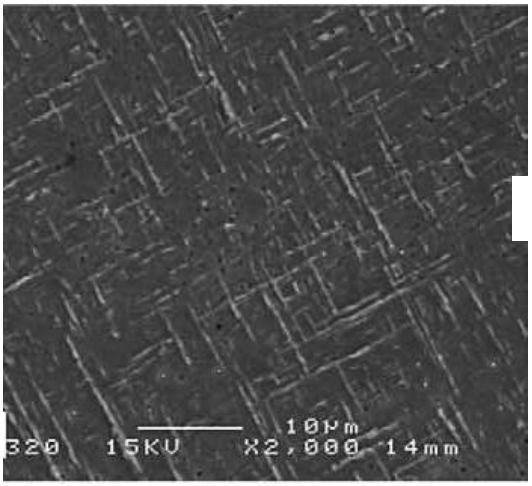

1-9b

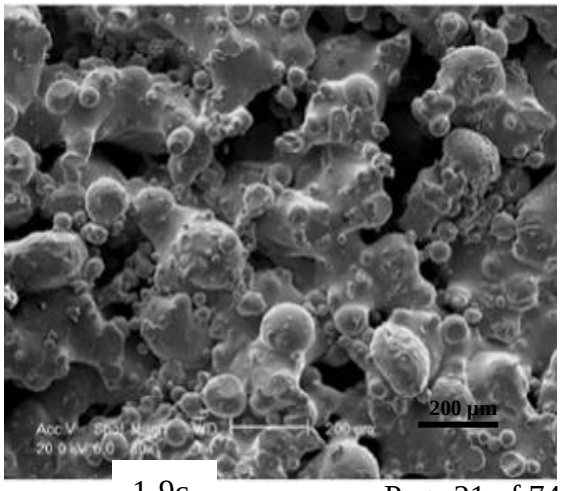

1-9c

Figures 1-9a to 1-9c : SEM images showing Ti–6Al–4V parts manufactured using DLF; SEM micrographs showing different microstructures produced at different laser powers of (a) 390W, (b) 264W and (c) 180W. The best microstructure has been achieved at 264W at a powder feed rate of 6 g/min, scan speed of 200 mm/min and Z-increment of 0.3 mm. [31]

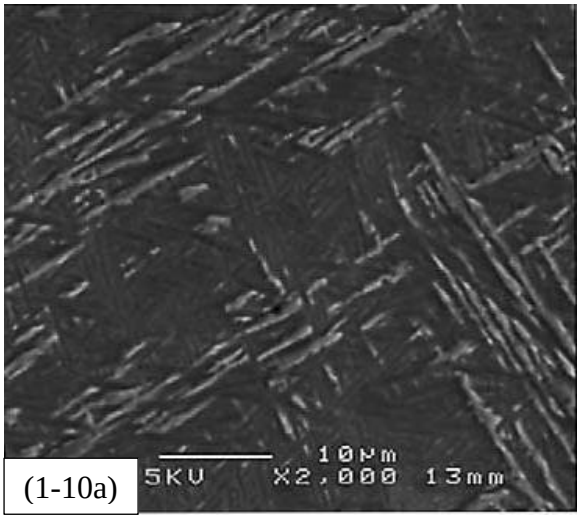

(1-10a)

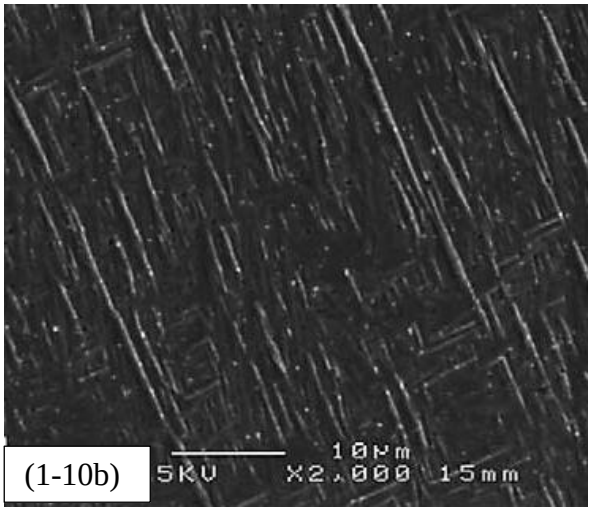

(1-10b)

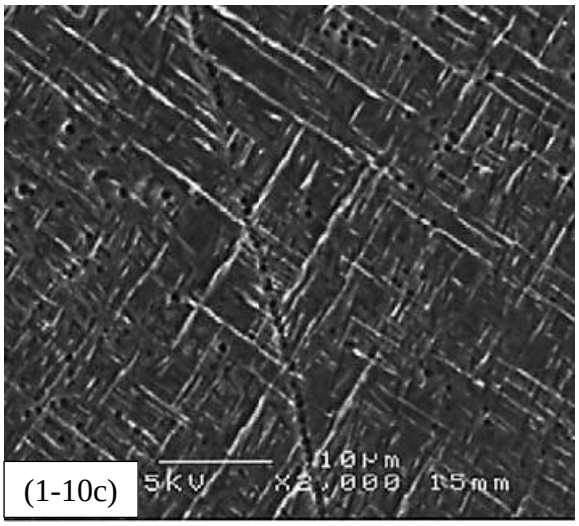

(1-10c)

Figures 1-10a to 1-10c: Secondary electron SEM micrographs showing the microstructures obtained at various laser scan speeds of (a) 600 mm/min, (b) 200 mm/min and (c) 900 mm/min at a laser power 432 W, a powder feed rate of 18 g/min, and a Z-increment of 0.3 mm. [31]

It has been concluded that the speed of 350 mm/min would produce the finest microstructure and increase or decrease of the scanning speed would significantly affect this microstructure.

An important process characteristic in the DLF is the height achieved against the theoretical height (as predicted). P.A. Kobryn &*et al*. study [38] on the effect of laser power and traverse speed on the build height of DLFed Ti-6Al-4V suggest the build height decreases with increasing the traverse speed on both thin and thick substrates. Their results agree with the results achieved in the study presented here.

In contrast, other studies [39,40] on the development of DLF structures suggest that the laser power has a critical level which once exceeded, there would be inadequate powder to adequately utilise the laser power and subsequently the build height will not increase with the increase of the laser power. The results presented in those studies also show that increasing the laser power would not necessarily develop the correct height unless flow rate is adjusted accordingly. The results achieved in this present study without establishing a critical laser power, conform to those discussed in the above mentioned studies.

1.7 Powder manufacturing method

Although this project will not engage with the manufacturing methods of the powder, two common metal powders manufacturing methods of PREP ® and Gas Atomisation have been reviewed as part of the literature review.

PREP® powder: PREP ® process stands for Plasma Rotating Electrode Process. This method of producing metal powder method is developed by Starmet Corporation and US patent has been granted. In the PREP ® method, the feedstock, (Ti) is used in the form of a rotary bar which is arced with gas plasma to melt. The molten metal is then centrifugally flung off the bar that forces it to cool down. The powders that are produced by this method are spherical; usually between 100 and 300μm in size, with good packing and flow characteristics that make this type of powder ideal for producing high quality, near net shapes products through methods such as HIP and DLF that can be used in variety of applications such as aerospace flying parts and porous coatings on HIP prostheses.

The PREP® method has several inherent characteristics that make the method uniquely suitable for the fabrication of specific alloy powders to provide manufacturing and product advantages. Firstly in PREP® method, the melting and atomisation stages are contactless and the powder produced achieves the

highest possible levels of cleanliness. The cleanliness is a critical aspect for reactive and high-melting-temperature alloys that are excessively corrosive in their molten form and attack conventional ceramic crucibles. Such alloys are routinely atomised by PREP® without picking up any contamination during the manufacturing process.

Also because PREP® atomisation is produced by centrifugal forces in contrast to aerodynamic drag of Gas Atomisation process, the powder is essentially free from porosity when compared to gas atomised powder.

Gas atomisation: In gas atomisation powder processing method, the metal melting in a vacuum induction furnace in water cooled copper crucible. The metal is tapped and the molten metal flows as atomised with a stream of high pressure inert gas. The small droplets once cooled, are very close to spherical shape and usually measure between 50 and 350µm. The Gas Atomisation process is currently being used to produce a wide variety of materials such as commercially pure (CP) titanium as well as conventional alpha-beta and beta alloys etc. Figure 1-11 shows a schematic diagram of the GA process.

A recent comparative study [32] using two different methods of Gas atomisation (GA) and the Plasma Rotating Electrode Process (**PREP**®) of Ti 6-4 powders. DLFed characteristics in terms of layer geometry, surface finish, microstructure and micro hardness and internal porosity were compared under similar process conditions.

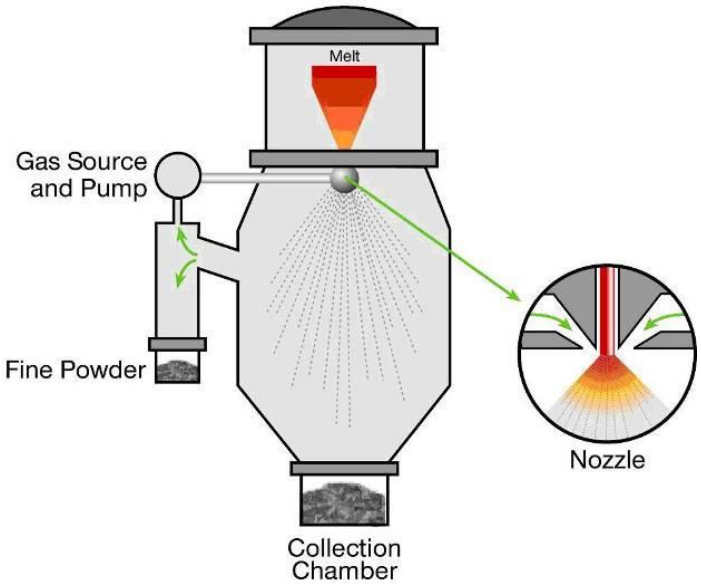

Figure 1-11: Typical Gas atomised process showing nozzle for streaming the molten metal, inert as source and powder collection chambers. Picture courtesy of LPW Technologies.

In other studies [33] the laser diffractometer results showed that the PREP® powder had, on average, smaller particles than the GA powder. The mean particle diameter was found to be 94µm for GA powder and 72µm for PREP powder. Figure 1-12a shows the PREP powder morphology which is highly spherical compared with the GA powder as shown in figure 1-12b.

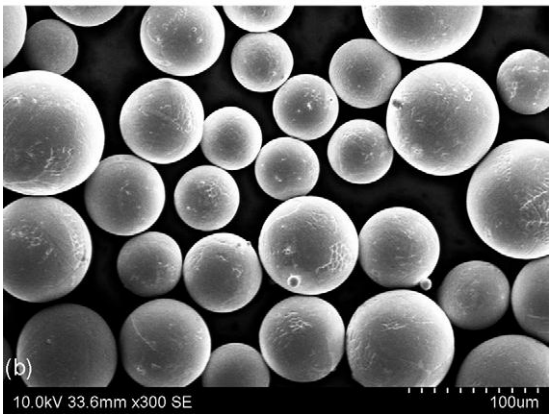

Figure 1-12a: SEM image of the PREP powder. Highly spherical particles. [31]

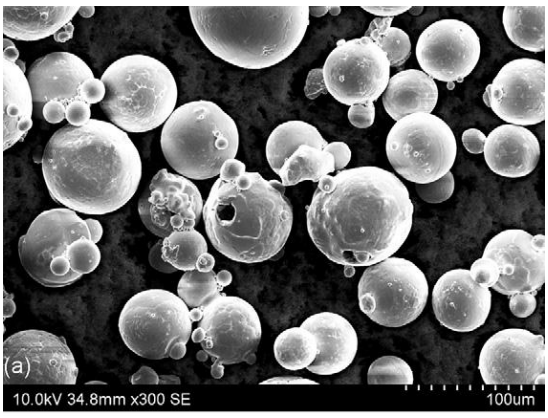

Figure 1-12b SEM image of the GA powder. Rough surfaces and approximate roundness of the particles compared to PREP powder in figure 7. [31]

In that study, Ti–6Al–4V blocks with a nominal size of 50 mm × 50 mm × 10 mm were used as substrates. Following the Design of Experiment practice, two levels of laser power and five levels of mass flow rate for each powder type were selected and tested at a constant scanning speed of 5 mm/s. 20 test runs for each family of powder were resulted from the test. The evaluation of the results reported the volumetric porosity in the PREP® powder to be three times less than the GA powder.

The study [33] also concludes that the structure of the DLFed structure in both cases is primary β grains and the size of the primary β grains tends to increase with the increase of laser power and reduced with decrease in the powder flow rate. Figures 1-13a and 1-13b show the changes in average size of primary β grains for GA and PREP fabricated samples with respect to mass flow rate and laser power.

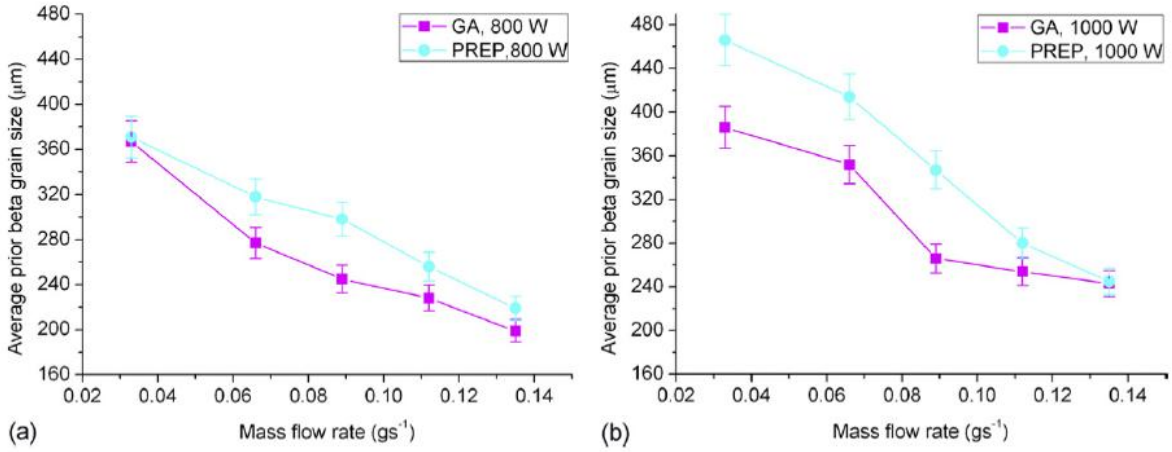

Figure 1-13: Average prior beta grain size of GA and PREP deposition samples compared as a function of mass flow rate: (a) Laser Power 800 W; (b) Laser power 1000 W [33]

1.8 Nozzles & Powder size

The direct laser deposition process is used for rapid fabrication of fully dense components with good metallurgical properties. As described before, in this process, the powder is usually fed into a laser focal point to create a pool of

molten metal, which solidifies rapidly once the laser beam moves away. One of the important issues of this process is the understanding of how the material powder is supplied to the deposition surface since the physics of this process affect and change the particle utilisation efficiency, fabrication dimensions, and even the final properties of the product.

Studies have been carried out on the distribution of powder stream. *Y.C.Fu et al.* studied [34] the interaction between powder particles and the laser and reported that the powder particles hit the surface at various temperatures as the result of varying times being exposed to the laser power and also different the variation of the laser power in the flow path. Jehnming Lin [39] developed a numerical model of focused powders suggesting that the powder concentration will decrease with the increase of gas flow velocities. Other study has also been carried out to better understand and clarify the importance of the nozzle arrangement and gas flow setting to powder concentration [30] and proposed a numerical model of coaxial powder flow for the DLF process. The study shows that numerical models can satisfactorily predict the deposition zone according to the local particle concentration and laser intensity distribution.

The numerical model in the study showed that the powder stream begins to expand at the exit point of the nozzle as the result of gravity and the mixed flow field of inner and carrier gases. The particle streams from all nozzles merge into a main stream to form a waist, at the distance below the nozzle tip. After travelling further away from the nozzle, the main stream of powder diverges, because the particles flow in different directions naturally. According to the characteristics of the powder stream structure, the powder flow below the nozzle may be categorised into three separated stages, pre-waist, waist, and post-waist, which are shown by zones a to c, respectively, in Figure 1-14.

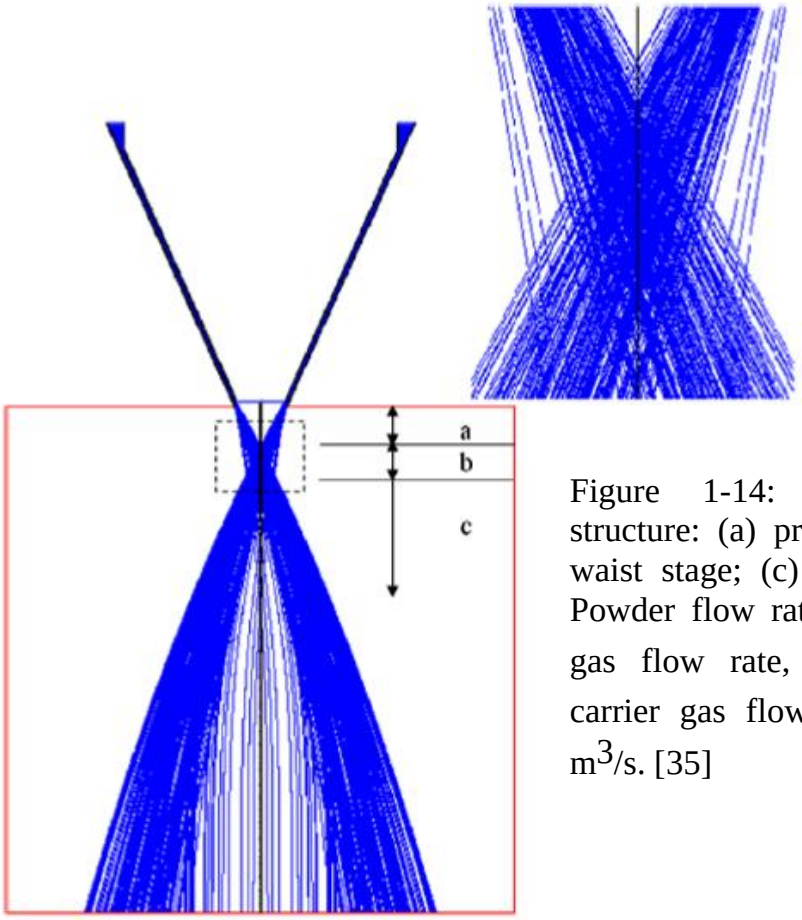

Figure 1-14: Particle stream structure: (a) pre-waist stage; (b) waist stage; (c) post-waist stage. Powder flow rate, 3 g/min; inner gas flow rate, 7.86×10^{-5} m^3/s; carrier gas flow rate, 7.86×10^{-5} m^3/s. [35]

In addition to the powder stream, another important result from the study was the powder heating process. The models predicted the powder temperature profile to be as indicated in Figure 1-15 by the vertical colour transition. The study suggests that the particles experience a rapid increase in temperature at the moment they enter the laser-particle interaction zone. The particles are quickly heated up from room temperature even up to 2000ºK or higher when passing through the laser irradiation zone.

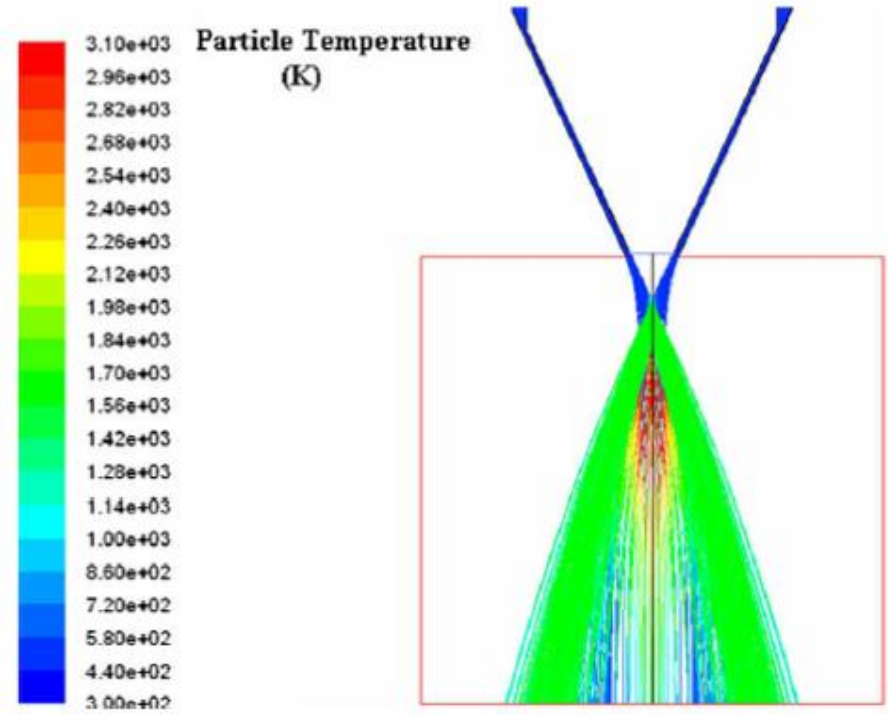

Figure 1-15: Powder jet temperature profile. Laser power, 300 W; beam diameter, 1.5 mm; powder flow rate, 5 g/min; inner gas flow rate, 7.86 X 10^{-5} m^3/s, carrier gas flow rate. [35]

1.9 Summary of Literature Review

The literature reviewed for conducting this study indicated that limited studies have been carried out on the metallurgical aspects of Titanium Ti-5553 and even less researches have been conducted on the DLF process of this alloy. Studies carried out on the heat treatment of Ti-5553 material suggest that reduction of increase of the Solution treatment temperature has direct affect on the precipitation of α-phase within β-matrix.

From the review of the published literatures, it can also be concluded that many processing variables would influence the final results of the DLF process and optimised, thorough control of the laser and the powder feeding system is essential for the successful DLF process. However those processing parameters are not the same for different alloys and even form the same alloy in various geometries.

The microstructures of the DLF samples are significantly dependent on the thermal pattern of DLF process. The parameters affecting the thermal pattern are Laser power, Laser scanning speed and Powder feed rate.

Another parameter affecting the microstructure of DLFed samples is the nature of the powder used for the process. Air atomised powders due to the nature of their manufacturing process will carry inherent porosity which will influence the microstructure of the DLFed samples, whereas the PREP(R) powder would not contain the inherent oxygen problem and tends to alleviate or even eliminate the porosity presence within the microstructure.

2 Experimental Procedures

2.1 Materials

The powder used for this study was Ti-5553 PREP® manufactured by STARMET Corp, with 0.08% Carbon content. Due to initial unavailability of a Ti-5553 substrate, for the purpose of the experiments, strips of Ti-6Al-4V were used as a substrate and actual Ti-5553 were used at the second stage as described in sections 2-4 and 2-5.

Substrates were cleaned and degreased with Acetone then placed on the laser bed and fixed in position in order to minimise the distortion during processing. In order to avoid oxidation, the laser bed was then sealed and bagged off in order to create a protective atmosphere. The created chamber was then purged with Argon in order to reduce the Oxygen content below 5 PPM. The bead size was kept at 2.0 mm. This bead size was chosen in order to produce an acceptable build rate in a timely manner.

As mentioned above at this stage the base material was Ti-6Al-4V since the first aim of the study was to establish the deposition parameters and the effects of the substrate composition was not considered in this part of the investigation.

2.2 Ti-5553 Powder Characterisation

Figure 2-1 shows the PREP® powder that was used in this study. From microscopically evaluation of the powder as shown in figures 2-1(a & b) it can be seen that particles tend to have elongated grain structure and it can be concluded that grains are elongated at the preferred cooling direction during solidification. The equiaxed grains as seen in figure 2-1b can be attributed to the plane of view and can be attributed to the elongated grains as seen in figure 2-1a which have been cut in the direction normal to the growth direction.

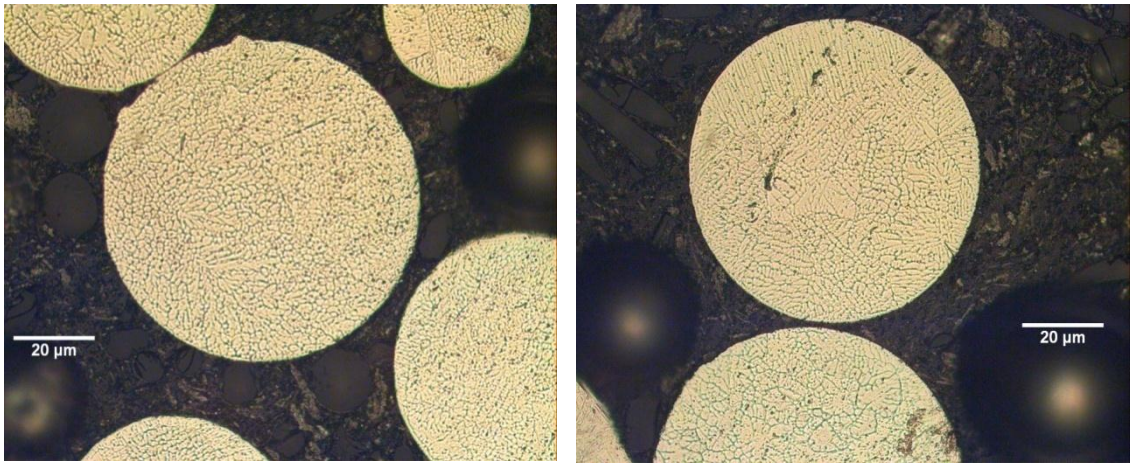

Figure 2-1: (a) on the left shows the equiaxed grain structure of the particles. (b) On the right shows elongated grains.

Powder analysis results (as shown in appendix A) showed the 80% of the powder is in size range of 70-120µm with the maximum concentration of particles within 100-120µm. The analysis was carried out on a sample of powder using the Laser Scattering particle size analyser (Beckman Coulter model - LS32) at the University of Birmingham.

SEM analysis was carried out on the powder used for this report. The SEM equipment was a ZIESS ® MICA EVO as shown in figure 2-2 operating at the nominal 20.0 KV.

Figure 2-2: SEM equipment used for this report.
Picture courtesy of Messier-Dowty Ltd.

The SEM analysis of the powder showed the particles were solidified without segregation as shown in figure 2-3. The images showed impressions on the particles, which can be the result of the particles impacts during solidification.

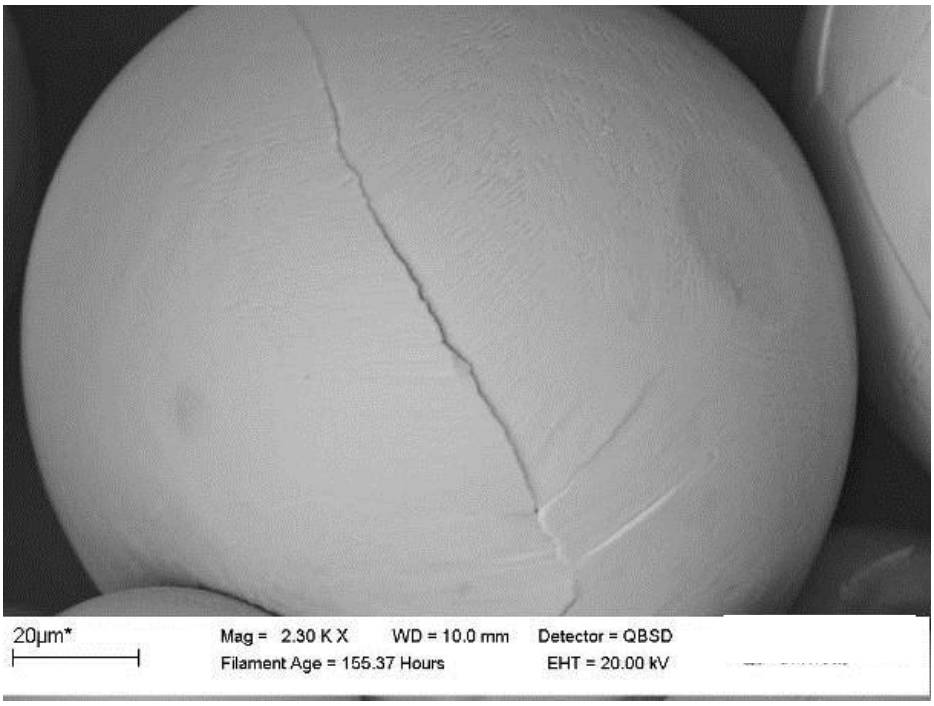

Figure 2-3: Backscattered electron micrograph of the same particle. The image shows grain boundaries

SEM analysis also showed that the particles are individual without satellites. This is shown in figure 2-4. Further analysis of the powder used in this study is given in Appendix A. A number of broken particles could be seen in the image that can be attributed to the fact that the powder had been used in the past and was recycled. The SEM results were comparable with those reported by other studies. [32]

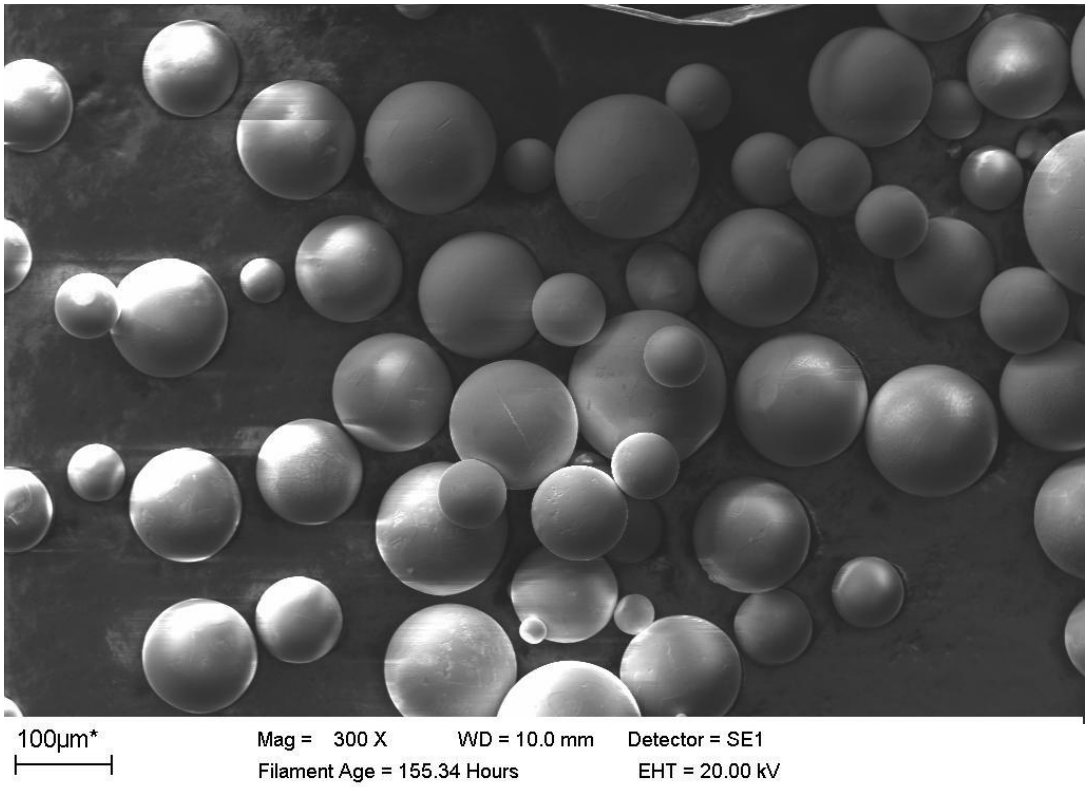

Figure 2-4: SEM Image of Ti-5553 powder used in this study. The image shows the particles are highly spherical and very fine surface.

2.3 Direct Laser Fabrication

For the efficient application of DLF, it is paramount that all important process parameters that could potentially affect the DLF process outcome be identified and the level of sensitivity of the operating conditions to these process parameters to be characterised.

Following the review of the previous work on DLF process as described in the literature review section, it has been concluded that the main parameters affecting the outcome of DLF process with a constant "Z" value are: **1) Laser Power**, **2) Powder Feed Rate** and **3) Scanning Speed.**

In the present work, a TRUMPF VFA 600 CO2 laser unit with power output 0 - 2000Watts and a Sulzer Metco type 9MPE closed loop powder feed unit with capacity of 1-100gr/min as shown in figure 2-6 was used. A "NUM 1060M" CNC unit is used to control the workstation and the laser beam movement. Figure 2-5 is the actual image of the DLF equipment used in this study. The laser beam is directed to the deposition region using a 5-inch focal length convex lens. The powder is injected through a 3-beam nozzle directly into the focused laser beam and the laser delivery column and powder nozzle move as an integral unit. An argon gas jet, coaxial with the beam axis, was used to shield the melt pool from oxidation. During the laser fabrication process the shielding gas pressure was kept constant.

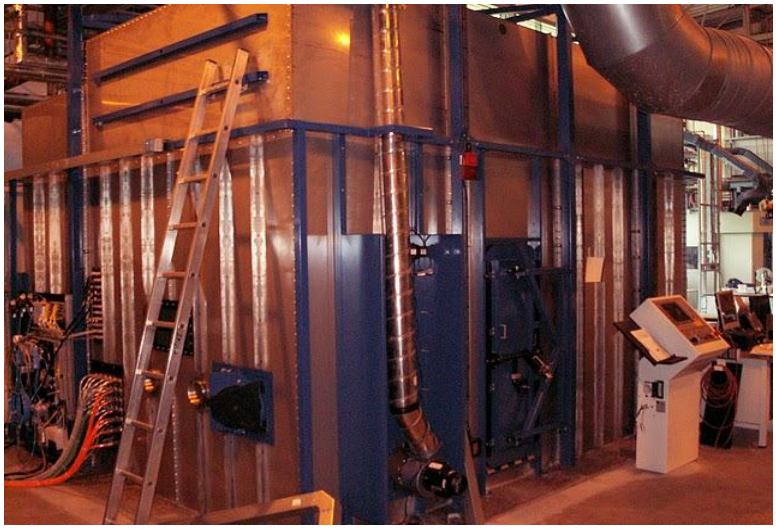

Figure 2-5: TRUMPF VFA 600 used in the present study. The instrument consists of the laser head and the nozzle attached to a CNC head enclosed in the chamber and the controller unit with the peripheral hardware for producing the deposition program and tool path.

The laser spot size at the focal point was 3½ mm dot and each pass had an overlap of 1½ mm with the previous pass. Other operating parameters were adjusted accordingly as described in section 2.3. Figure 2-6 shows the 3-beam nozzle as used in this experiment.

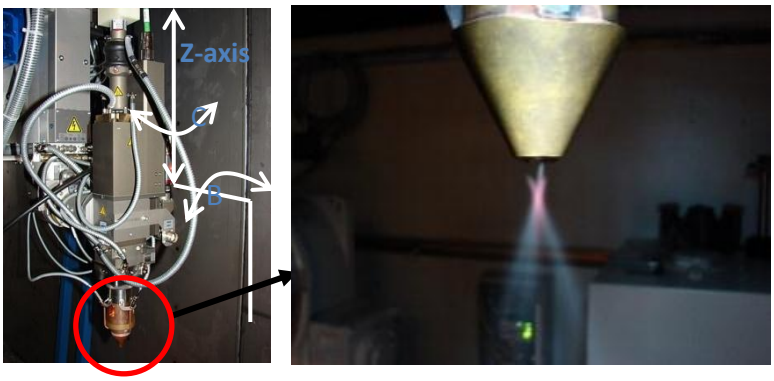

Figure 2-6: The 3-beam nozzle used for this experiment. Figure on the right is magnified to show the actual nozzle tip. Picture courtesy of the University of Birmingham, School of Metallurgy & Materials.

2.4 Preliminary Studies

In order to better understand and investigate the effects of processing parameters of the microstructure and mechanical properties of the DLF produced structures, experiments were designed using Factorial Experimental methodology.

A Factorial Design looks at the effects of varying the levels of different factors that would affect the process output. Each complete experiment or replication of the experiment accounts for all the possible combinations of the varying levels of those factors. Once implemented satisfactorily, the Factorial Design ensures that the maximum amount of data on the effect on the process output has been achieved through the minimum number of experimental runs.

For example, if the effects of two factors X and Y on the output of a process are investigated, and X has 3 levels of intensity (i.e. Low, Medium, and High presence) while Y has 2 levels (Low and High), then only 6 treatment combinations runs are required to complete the experiment, covering the process output for each of the combinations:

Low X-Low Y,
Low X-High Y,
Medium X-Low Y,
Medium X-High Y,
High X-Low Y,
High X-High Y

In this research the factors as described earlier were considered as: **1) Laser Power**, **2) Powder feed rate** and **3) Scanning speed.** For each factor (variable) 3 levels have been considered: **Low**, **Medium** and **High**. The basic concept of design of experiment using Factorial Experiments methodology would result in 27 experiments

Prior studies carried out in 2010 at the University of Birmingham on Ti-5553 on behalf of Messier-Dowty Ltd had suggested a selection of process parameters which could produce an acceptable microstructure. These parameters have been considered as the Medium values for this study. Table 2-1 is the actual matrix which indicates the combination of the tests which have been carried out:

Factor 1: Laser Power	**Factor 2: Powder feed**	**Factor 3: Scanning speed**	**Test Reference**
Low: 20%	Low: 5 g/min	Low: 600 mm/min	Sample 1
Low: 20%	Low: 5 g/min	Medium: 800 mm/min	Sample 2
Low: 20%	Low: 5 g/min	High: 1000 mm/min	Sample 3
Low: 20%	Medium: 7 g/min	Low: 600 mm/min	Sample 4
Low: 20%	Medium: 7 g/min	Medium: 800 mm/min	Sample 5
Low: 20%	Medium: 7 g/min	High: 1000 mm/min	Sample 6
Low: 20%	High: 9 g/min	Low: 600 mm/min	Sample 7
Low: 20%	High: 9 g/min	Medium: 800 mm/min	Sample 8
Low: 20%	High: 9 g/min	High: 1000 mm/min	Sample 9
Medium: 45%	Low: 5 g/min	Low: 600 mm/min	Sample 10
Medium: 45%	Low: 5 g/min	Medium: 800 mm/min	Sample 11
Medium: 45%	Low: 5 g/min	High: 1000 mm/min	Sample 12
Medium: 45%	Medium: 7 g/min	Low: 600 mm/min	Sample 13
Medium: 45%	Medium: 7 g/min	Medium: 800 mm/min	Sample 14
Medium: 45%	Medium: 7 g/min	High: 1000 mm/min	Sample 15
Medium: 45%	High: 9 g/min	Low: 600 mm/min	Sample 16
Medium: 45%	High: 9 g/min	Medium: 800 mm/min	Sample 17
Medium: 45%	High: 9 g/min	High: 1000 mm/min	Sample18

High: 65%	Low: 5 g/min	Low: 600 mm/min	Sample 19
High: 65%	Low: 5 g/min	Medium: 800 mm/min	Sample 20
High: 65%	Low: 5 g/min	High: 1000 mm/min	Sample 21
High: 65%	Medium: 7 g/min	Low: 600 mm/min	Sample 22
High: 65%	Medium: 7 g/min	Medium: 800 mm/min	Sample 23
High: 65%	Medium: 7 g/min	High: 1000 mm/min	Sample 24
High: 65%	High: 9 g/min	Low: 600 mm/min	Sample 25
High: 65%	High: 9 g/min	Medium: 800 mm/min	Sample 26
High: 65%	High: 9 g/min	High: 1000 mm/min	Sample 27

Table 2-1: The experimental program developed based on Factorial Experiment Design methodology.

2.4.1 Stage 1: Ti5553 on Ti6Al-4V substrate

At the first stage, Ti-5553 powder was deposited on Ti-6Al-4V substrate due to unavailability of appropriate Ti-5553 substrate. Ti-5553 substrate were later made available and used as described in section 2.5.

At this first stage the following parameters were considered as shown in table 2-2:

Factor 1: Laser Power	**Factor 2: Powder feed**	**Factor 3: Scanning speed**	**Test Reference**
High: 65% (Average: 1290 W) 1168-1460 W 1.01 ms	Medium: 7 g/min – 3 RPM	High: 1000 mm/min	H.M.H
High: 65%	Medium: 7 g/min	Low: 600 mm/min	H.M.L
High: 65%	Medium: 7 g/min	Medium: 800 mm/min	H.M.M
Medium: 45% (Average: 890	Medium: 7 g/min	Low: 600 mm/min	M.M.L

w) 759 - 995			
Medium: 45%	High: 9 g/min	Low: 600 mm/min	M.H.L

Table 2-2: The first stage deposition was carried out using Ti-5553 powder and Ti-6Al-4V substrate. Each sample is identified with the applicable parameters setting.

Prior to start the process, the powder container was completely disassembled and thoroughly cleaned to remove the traces of the previous powder used. The container was then put back together and filled with Ti-5553 powder. In order to ensure all traces of the previous powder had been removed from the laser system, a burn out cycle was applied for a number of times and the results were analysed until the particle analysis system showed no trace of the previous powder.

The results of this stage are subsequently described and discussed in Section 3 of this report. It must be noted that the substrates were in form of strips of Ti-6Al-4V wit approximate size of 100mm X 40 mm. Samples were clamped onto the machine table under a sealed bag filled with Argon as the protective medium. Deposition process only started when the oxygen content inside the bag had reached below 5 ppm. Samples were produced in form of cubes with 20mm X 20mm X 20mm.

2.4.2 Stage 2: Ti5553 on Ti-5553 substrate

As mentioned earlier, at the initial test phase, a limited amount of PREP Ti-5553 powder was available for experiments. Due to the nature of the Ti-5553, the lead time for preparation of the powder is lengthy. Nonetheless further tests were continued once adequate amount of PREP Ti-5553 as well as appropriate substrates (Ti-5553 substrate) were made available. Ti-5553 plates were used as substrates as shown in figure 2-5. Similarly 20mm X 20mm cubes were deposited

on these substrates in pre-defined locations as shown in the figure 2-7. .

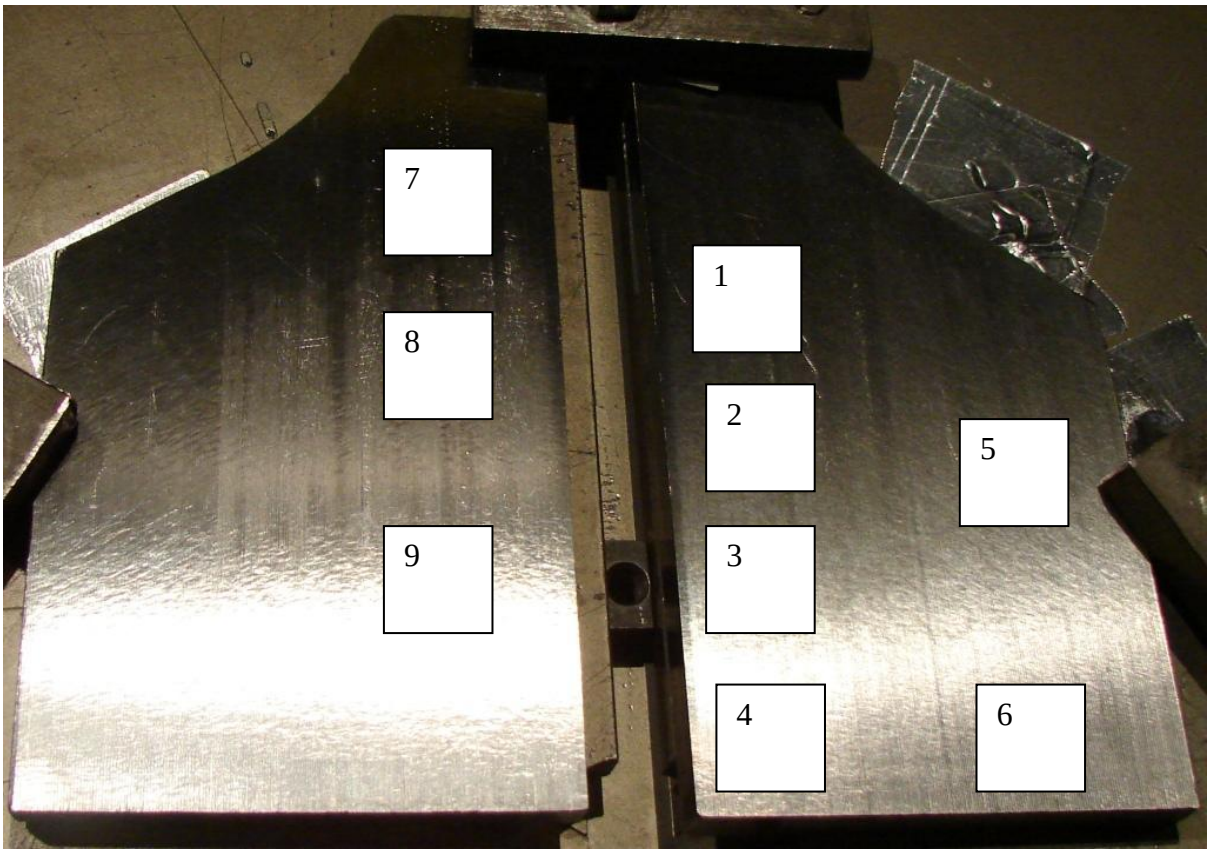

Figure 2-7: Ti-5553 substrates were prepared and clamped ready for sample deposition. Samples were deposited on the locations predefined as shown in this picture.

Substrates were cleaned and degreased with Acetone and then placed on the laser bed and fixed in position in order to minimise the distortion during processing. In order to avoid oxidation, the laser bed was then sealed and bagged off in order to create a protective atmosphere. The created chamber was then purged with Argon in order to reduce the Oxygen content below 5 PPM. The bead size was kept at 2.0 mm. The bead size was chosen in order to produce an acceptable build rate in a timely manner. The produced test samples are described and analysed in Section 3 of this report.

2.5 Optical microscopic evaluation

Once the DLF process was completed and the samples were produced, samples were measured for physical dimensions and suitable samples were selected. Select samples are identified in section 3 of this report.

The samples were sectioned off and polished and prepared for micro-analysis. The polishing process was carried out using an initial polishing using 400, 800, 1200 and 2500 mesh polishing pads. After this, samples were further polished using 3μ and 1μ diamond suspension and appropriate polishing pads.

Microstructural analyses were carried out using a Leica ™ optical microscope capability of 100X, 200X 500X & 1000X and Omnimet® image analysis software. The selected samples were viewed initially in unetched condition in order to detect any porosity within the deposition layers and then etched with Kroll's etchant.

2.5.1 Image analysis on micro-sections

In order to establish the volume fraction of precipitated alpha phase within the beta matrix, a contrast separation technique was used. The contrast thresholds on software Omnimet ® could be comfortably set to highlight the alpha phase on both base and deposition samples. The analysis results are shown in Section 3. For the samples to be viewed under optical microscope, once cut and mounted, the surface was prepared using 400, 800, 1200 and 1200 grade wet and dry rotating polish discs. The samples were further polished using 9μ and 3μ diamond polish.

To evaluate the microstructure of the samples, prepared samples were etched using Kroll's reagent. The etchant was made fresh each time the sample required etching. The typical chemical composition of the Kroll's reagent is 100ml water, 1-3ml Hydrofluoric Acid and 2-6ml nitric acid.

2.6 Mechanical tests on sectioned samples

Micro-hardness tests and tensile testing were carried out on the samples to establish the mechanical properties of the samples under various conditions as described in section 3. Details of these experiments are explained below.

2.6.1 Micro-hardness testing on deposited samples

Following the microscopic evaluation of the samples, sectioned off samples were subject to micro-hardness testing as described here.

Micro-hardness tests were carried out on the substrate and the deposited layers longitudinally and transverse as shown in figure 2-6 to establish the variation of hardness within the deposit and also for comparison purposes between the hardness of the base material away from the heat zone in contrast with the hardness of the heat affected zone. A Mitutoya microhardness tester with a load range of 3Kg was used for the hardness testing of the sample.

The hardness readings were taken from the base material away from heat affected zone, shown as zone (1) on figure 2-8 towards the deposition and including the HAZ.

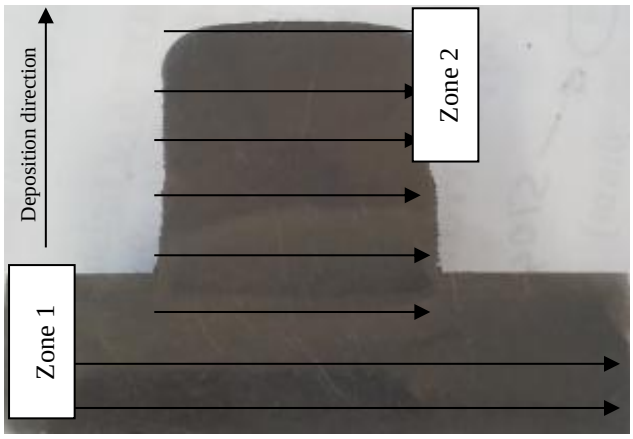

Figure 2-8: Hardness tests were taken as shown on this picture. Hardness tests were taken 2.0 mm apart. Each series were taken at 3.0mm above the previous set of readings.

2.6.2 Tensile test

Tensile tests were carried out to establish the mechanical properties of deposited material. For this purpose, test blocks were deposited and tensile test samples were extracted from those cubes. Test blocks were produced for both transverse and longitudinal testing directions. Figure 2-9 illustrates the test blocks that have been fabricated so the tensile test pieces can be extracted.

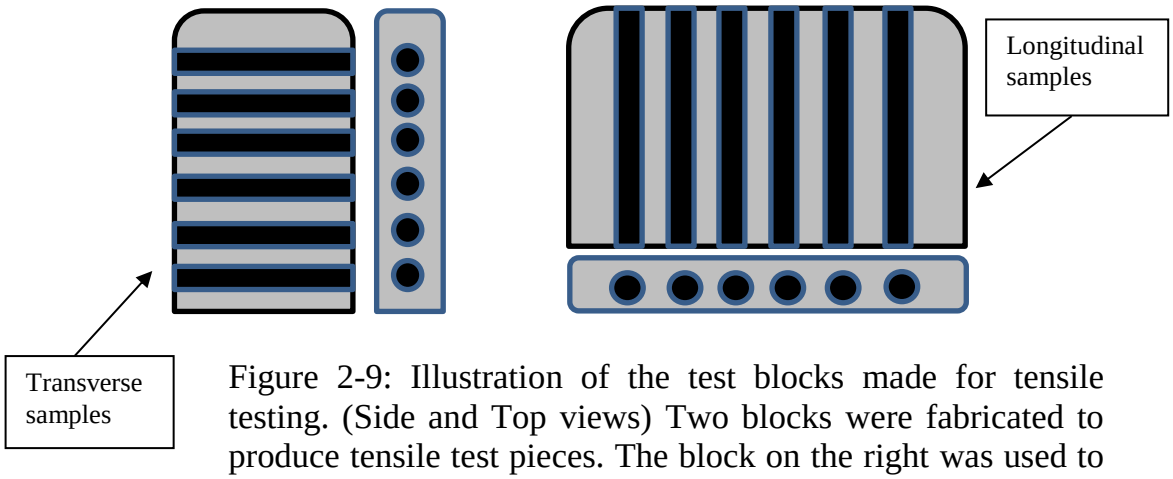

Figure 2-9: Illustration of the test blocks made for tensile testing. (Side and Top views) Two blocks were fabricated to produce tensile test pieces. The block on the right was used to extract vertical (longitudinal) test pieces and the block on the left was used for vertical (Transverse) test pieces. 8mm diameter test pieces were cut using wire-cut equipment.

Test pieces were cut through the test blocks with an initial diameter of 8mm using Agie Charmilles Wire-Erosion equipment. Longitudinal tensile test pieces were extracted parallel to “Z” direction and Transverse test pieces were extracted in “Y” direction. Test pieces were initially produced using the wire-erosion machine and then machined off to the final dimension. Those samples that were subject to further heat treatment, were machined off after the relevant heat treatment cycles as described in section 3.6.1 & 3.6.2 of this report were completed. Round test pieces were machined off to meet the requirements of ASTM E8 and Messier-Dowty PCS 1003 [36] as per drawing number 100028955, with a gauge diameter of 3.96mm and the overall length of 60mm. Drawing for this test piece is available in PCS1003 [36].

Machined test pieces were then tested using a 100KN Denison-Mayes tensile tester with 0-25 mm extensometer in accordance with ASTM E8. The tensile tester is equipped with rate controller and the Stress/Strain curve was drawn automatically. Further analyses are described in section 3 of this report.

The actual tensile test results are shown in Appendix C.

3 Process Analysis and Discussion

3.1 DLF of Ti-5553

This initial study was arranged in order to eliminate the combination of the test parameters which would produce unacceptable test results. The purpose of this study was to identify the acceptable processing parameters for further research. At this stage, due to unavailability of Ti-5553 substrates, Ti-6Al-4V substrates were used. Once the substrates were clamped on the work table, the entire setup was shielded by the protective bag filled with Argon gas to remove any traces of Oxygen.

DLF machine was setup to produce 20mm X 20mm X20mm cubic samples as per table 3-1 settings. The setting parameters were selected to represent the possible extreme conditions for each setup possibility.

Sample ID	**Factor 1: Laser Power**	**Factor 2: Powder feed**	**Factor 3: Scanning speed**
HMH	High: 65% (Average: 1290 W) 1168-1460 W	Medium: 7 g/min	High: 1000 mm/min
HML	High: 65%	Medium: 7 g/min	Low: 600 mm/min
HMM	High: 65%	Medium: 7 g/min	Medium: 800 mm/min
MML	Medium: 45% (Average: 890 w) 759 - 995	Medium: 7 g/min	Low: 600 mm/min
MHL	Medium: 45%	High: 9 g/min	Low: 600 mm/min

Table 3-1: The first 5 samples were deposited on the Ti-6-4 substrate due to unavailability of the T-5553 substrate.

Following the deposition stage, table 3-2 shows the outcome of the first series of fabrication on the Ti 6Al-4V substrates.

Sample ID	Deposition height achieved	Result	Considered further?
HMH	6.6mm after 20mm deposition	Cube 1 - Failure	No
HMM	13mm after 20mm of deposition	Cube 3: Height low	No
HML	20mm after 20mm deposition	Acceptable	Yes
MML	10m after 20mm of deposition	Cube 4: Height low	No
MHL	20mm after 20mm of deposition	Cube 5	Yes

Table 3-2: The first deposition stage carried out using Ti-5553 powder on Ti 6Al-4V.

The height of the samples was measured using a calibrated 0-200mm Mitutoyo caliper to an accuracy of 0.01mm. The heights were measured from the highest point of the built to the top surface of the substrate. The measuring method was repeated throughout the project for all samples.

3.2 Observation after the first DLF stage:

This section only describes the observations and evaluation of the successful and acceptable samples following the deposition stage.

- Sample HML: The sample was considered as a success. The actual height of 20 mm was correct compared to the theoretical height of 20 mm. The sample was considered for metallographic evaluation.
- The sample was considered successful with some drawbacks as described below:

Due to the restriction on the machine bed, inadequate clamping was applied to the base material. As a result, significant distortion was developed on the base metal. Figure 3-1 shows the distortion of the sectioned off sample.

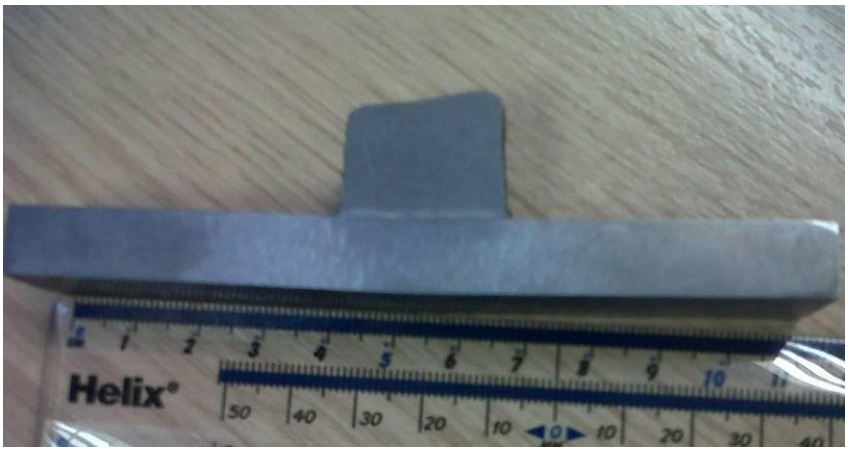

Figure 3-1: The distortion on the base-metal due to inadequate clamping on the sample. This deformation shows the importance of clamping down the substrate prior to deposition.

This issue highlights the importance of adequately holding down the substrates during the deposition stage.

3.3 Ti-5553 deposition of Ti-5553 substrate:

As mentioned earlier, at the initial test phase, a limited amount of PREP Ti-5553 powder was available for experiments. Due to the nature of the Ti-5553, the lead time for preparation of the powder is lengthy. Nonetheless further tests were continued once adequate amount of PREP Ti-5553 as well as appropriate substrates (Ti-5553 substrate) were made available. Ti-5553 plates were used as substrates as shown in figure 3-2. Similarly 20mm X 20mm cubes were deposited on the substrates in pre-defined locations as shown in the figure 2-7.

As described in section 2, the experimental program was defined in table 2-1. Starting from sample LLL (S1), figure 3-2 shows that the produced cube did not adhere to the substrate. This is due to inadequate heat input into the substrate. As the result, the surface of the substrate was not melted. Subsequently all

experiments with the laser power set as Low (S1-S9) was cancelled and considered as invalid.

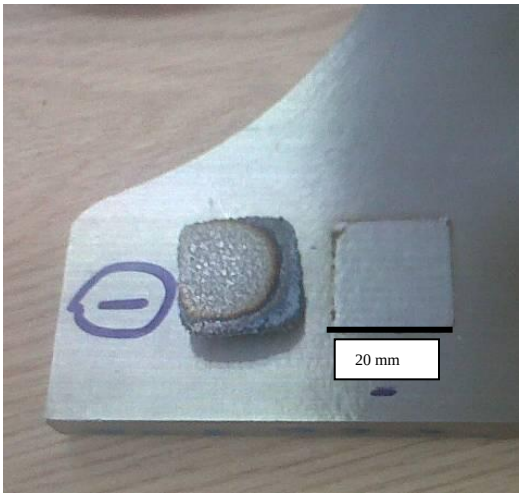

Figure 3-2: The cube is detached from the surface. Further visual examination showed no melting has occurred on the surface of the substrate at 20% laser power. All tests with low (20%) laser power were subsequently cancelled and deleted from the test program.

Deposition on Ti-5553 substrates was carried out as summarised in table 3-3. Each cube was deposited separately before the nozzle moved to the next deposition location.

Sample ID	**Deposition height achieved**	**Result**	**Considered further?**
M.L.L (Sample 10)	9.3mm after 20mm deposition	Unacceptable	No
M.L.M (Sample 11)	4.0mm after 20mm deposition	Unacceptable	No
M.M.L (Sample 13)	10mm after 20mm deposition	Unacceptable	No
M.H.L (Sample 16)	20mm after 20mm deposition	Acceptable	Yes
M.H.M (Sample 17)	10mm after 20mm deposition	Unacceptable	No
H.L.L (Sample 19)	10mm after 20mm deposition	Unacceptable	No
H.M.L (Sample 22)	20mm after 20mm deposition	Acceptable	Yes
H.M.M (Sample	13mm after 20mm	Unacceptable	No

23)	deposition		
H.M.H (Sample 24)	6.6mm after 20mm deposition	Unacceptable	No
H.H.L (Sample 25)	22.5mm after 20mm deposition	Acceptable	Yes
H.H.H (Sample 27)	22.5mm after 20mm of deposition	Acceptable	Yes

Table 3-3: Deposited samples were made using 3 levels of each processing parameter and the results of height achieved after 20 mm nominal deposition layers. Only those samples that achieved the correct height have been considered for further analysis.

3.4 Dimensional evaluations and analysis:

Following the completion of the deposition of all above samples, dimensional measurements were carried out to establish the correlation between the processing parameters and the height of deposition. For this purpose, samples were sectioned through from the highest point and the distance between the highest point of the build to the bottom face of the substrate were measured using a calibrated 0-200mm Mitutoyo calliper with an accuracy of 0.01mm. This method has been used on all samples.

Since the lowest laser power did not produce enough heat to melt the surface of the substrate, the experiments stated with 2 laser settings: Medium @ 45% of the power with an average of 890 Watts and High @ 60% of the maximum output with an average of 1460 Watts. Data gathered and shown in figure 3-3 for laser power setting at 45% and 3-4 for the laser power set at 60%.

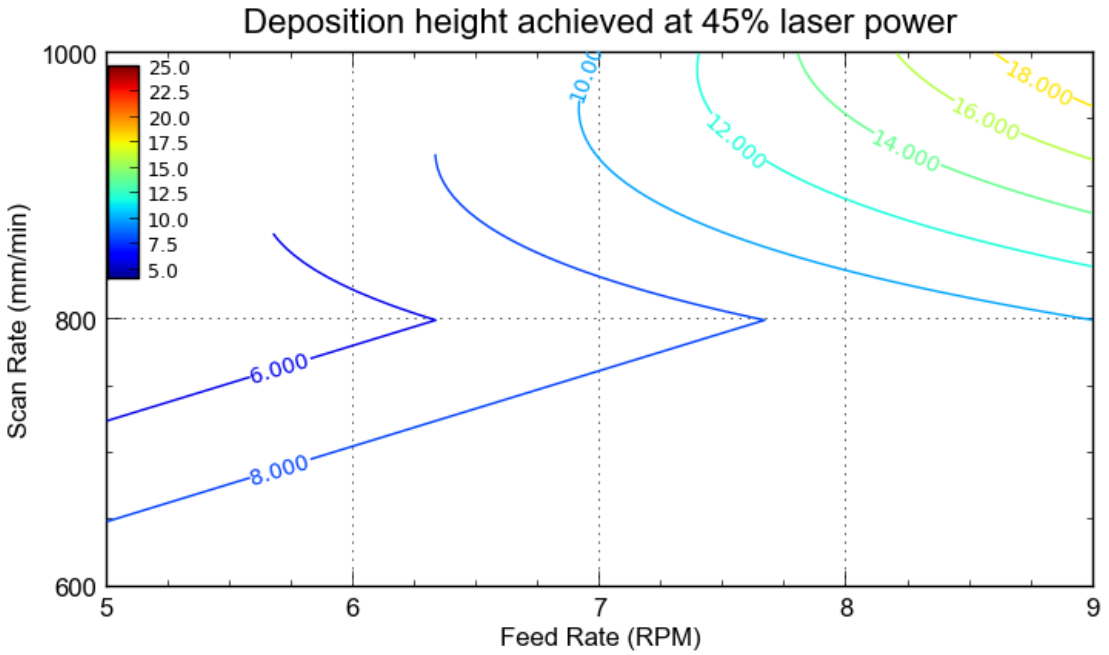

Figure 3-3: The graph shows the correlation between the Final achieved height as the result of Feed Rate and Scan Speed with a constant laser power of 45%.

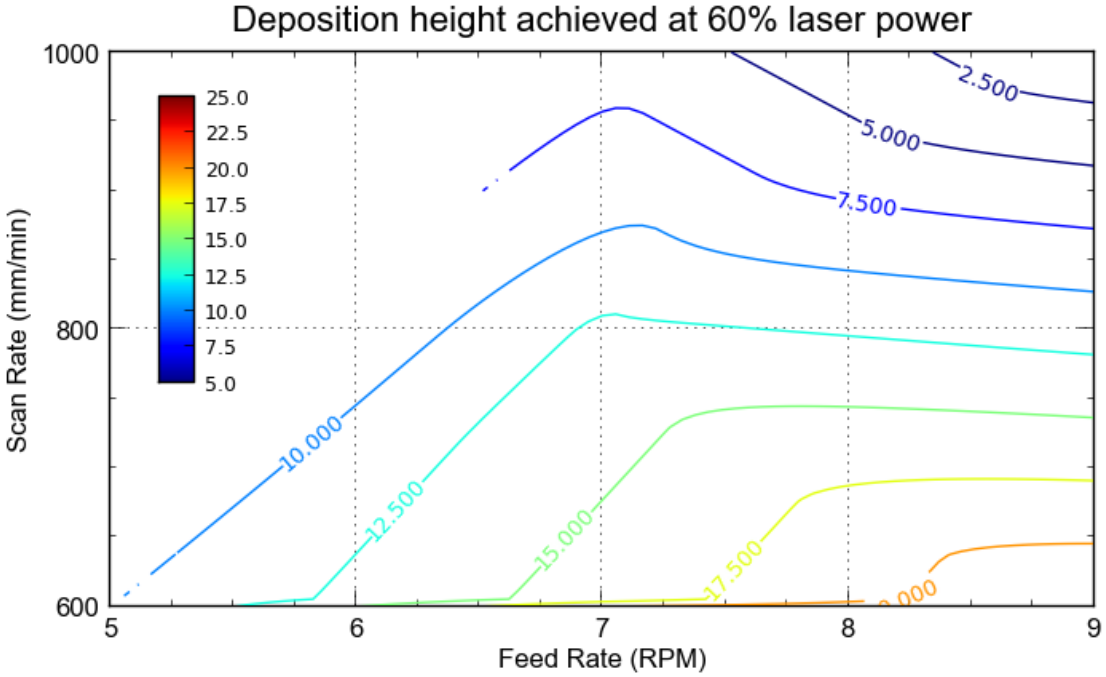

Figure 3-4: The graph shows the correlation between the Final achieved height as the result of Feed Rate and Scan Speed with a constant laser power of 60%.

It must be noted that based on the extrapolation of each unacceptable condition, other combination of the processing parameters where based on the information from the literature review or extrapolation of the result would predict unacceptable results were taken off the program and not included.

Further evaluations were carried out on the acceptable samples # 16, 22, 25 and 27 for the level of spattering around the deposition layers, the geometry of the build, defect build-up during deposition and processing time. Processing parameters H.H.H (Sample #27) was considered the satisfactory combination of the parameters.

3.5 Microscopic Evaluation:

The selected sample was sectioned off and prepared as described in section 2. The prepared section was viewed for porosity and other manufacturing defects within the layers in unetched condition, and then it was etched for micro-structural analysis.

3.5.1 Microscopic analysis of unetched sample:

One of the important aspects of this research is to establish the level of porosity within the build and even more significantly, within the interface of the deposition and the substrate. Microscopic evaluation of the deposited layers as shown in figure 3-5 show no porosity contained within the microstructure. Further analysis of the microstructure also showed no inter-layers defects such as lack of fusion or lamination.

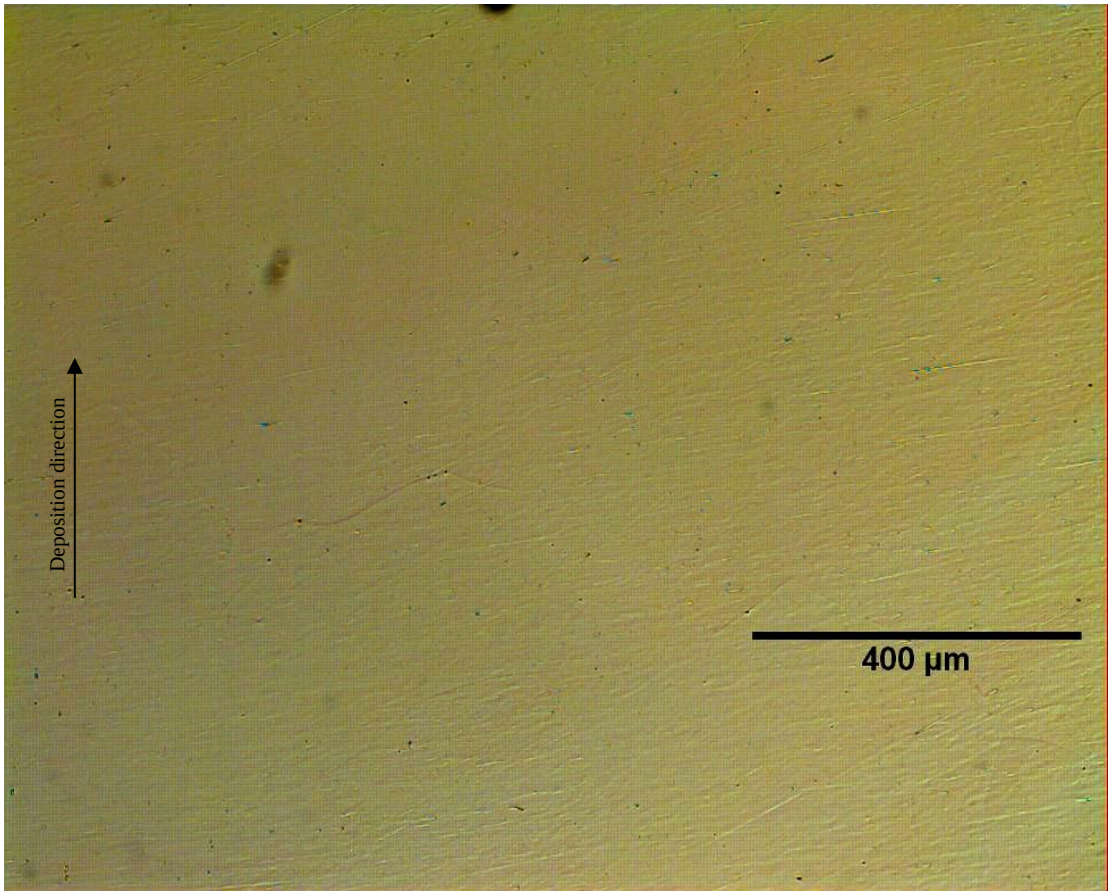

Figure 3-5: Micro-section of deposited layers of Ti-5553. No porosity or interlayer defects can be seen. The microstructure appeared solid and fully integrated without any interlayer defects.

Further analyses were carried out to establish if any defects have been formed between the substrate and the deposited layers. Figure 3-6 shows the unetched section of the interface between the substrate and the deposition. As shown in this image the interface also appears without any defects. The Heat Affected Zone can be seen due to the different crystallographic arrangements of the grains in this area and the adjacent areas.

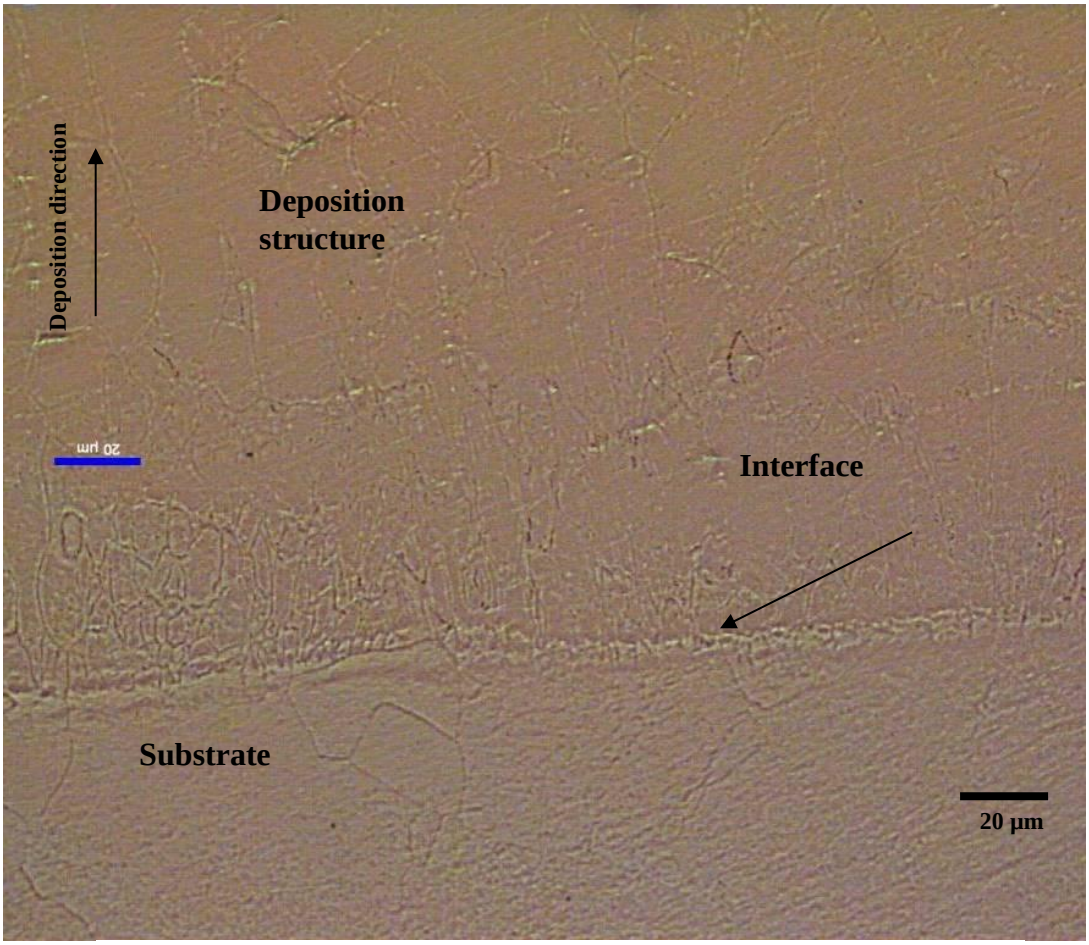

Figure 3-6: The image taken from the interface between the substrate (at the bottom) and the deposited layers (at the top). Similar to the actual deposit, here also no sign of porosity or other defects can been seen.

Comparisons were made between the micro section of the substrate and the deposition in order to highlight any immediate differences between the two. In the unetched condition, it is not possible to observe the exact microstructure including the grain boundaries and α and β phases. However at the higher magnifications, it was noted that Ti-5553 substrate showed a considerable amount of precipitates with smooth edges as shown in figure 3-7 when compared to what seemed to be precipitates in as-deposit with needle type precipitates shown in figure 3-8, all appeared white in a dark background.

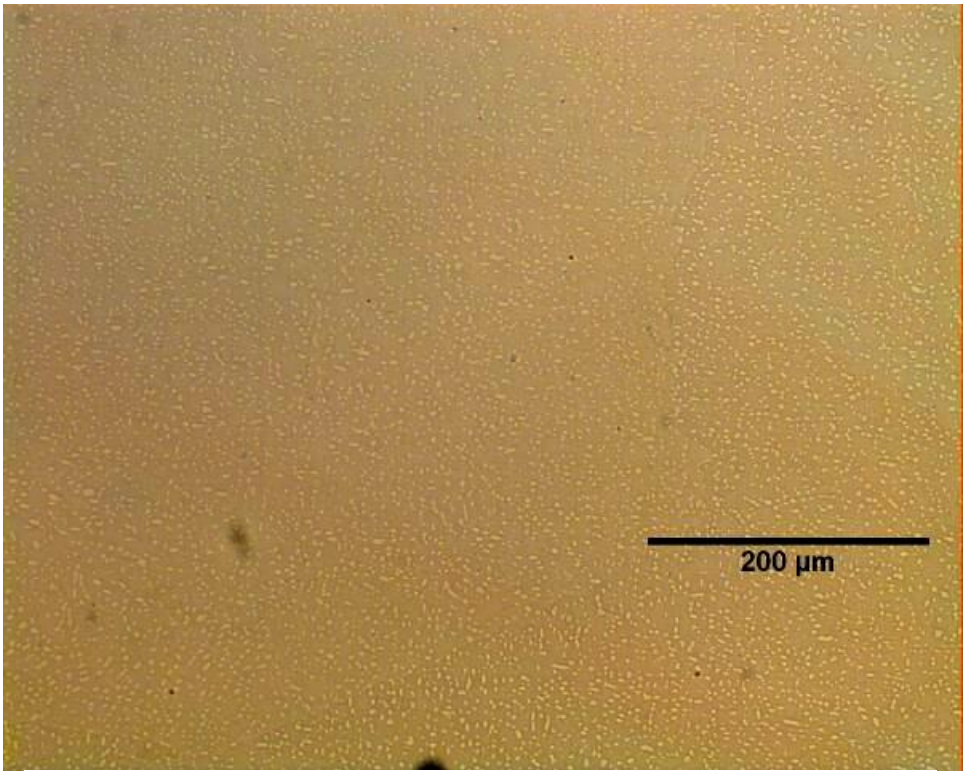

Figure 3-7: Substrate micro-section does not show any grain boundaries however very small precipitates can be seen evenly dispersed within the material. The precipitates have smooth edges and cylinder shape.

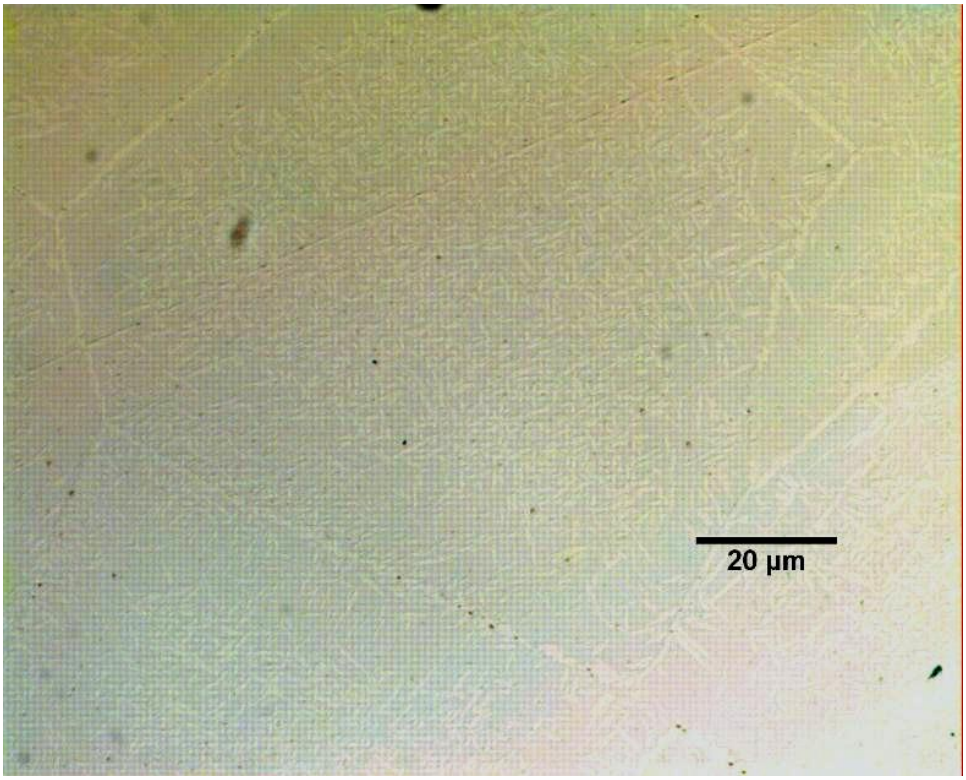

Figure 3-8: As-deposit micro-section shows a shade of grain boundaries with needle type precipitates dispersed within and the edges of the grains.

3.5.2 Microstructural analysis of DLF samples – Etched

Following the visual and micro-evaluation in unetched condition, the samples were etched with Kroll's etchant and dried off. The microstructural analysis was carried out on both categories of test pieces: Ti-5553 deposition on Ti-6Al-4V and Ti-555-3 deposition on Ti-5553 substrate.

3.5.2.a – Microstructural evaluation of Ti-5553 deposition on Ti-6Al-4V substrate:

Figure 3-9 shows the microstructure of the Ti 6Al-4V substrate in contrast with the microstructure of the deposited Ti-5553 taken from sample HML during the first stage of the experiment.

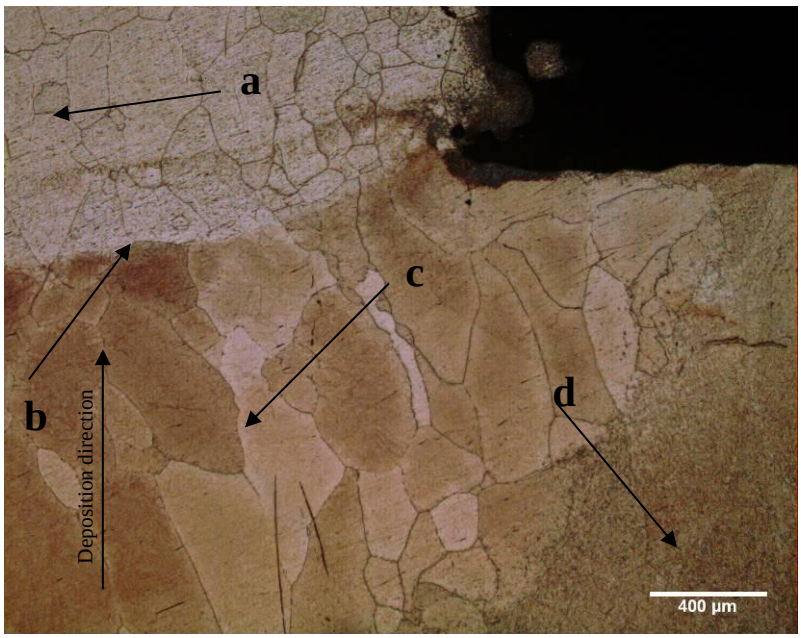

Picture 3-9: (a) Deposition layers of Ti-5553 powder, (b) deposition interface, (c) Heat affected zone which has been re-crystallised & (d) unaffected base metal.

As mentioned before, Ti-6Al-4V has been used as a substrate since the appropriate substrate was not available. The metallurgy of this alloy is not reviewed and researched in this report. The figure illustrates the Heat Affected zone and the microstructural changes due to the heat input form the process and the boundary between the deposition and the substrate.

3.4.2.b - Microstructural evaluation of Ti-5553 deposition on Ti-5553 substrate:

Ti-5553 deposition on Ti-5553 substrate was also subject to metallographic evaluation after etching. Figures 3-10 and 3-11 show the grain growth throughout the deposition as moving away from the deposition/substrate interface. This growth is associated with the increase in residual heat build-up as deposition progresses. The grains measured within 250-600µm and appear as equiaxed.

Ti-5553 substrate as shown in figure 3-12 contains significant volume of α-phase precipitated during the thermal processes at the forging stage and subsequent to the thermal treatments at the later stages during the manufacture. In contrast, as illustrated by figures 3-10 and 3-11, the as-deposited microstructure contains 100% β-grains and no chance has been given to α-phase for precipitation.

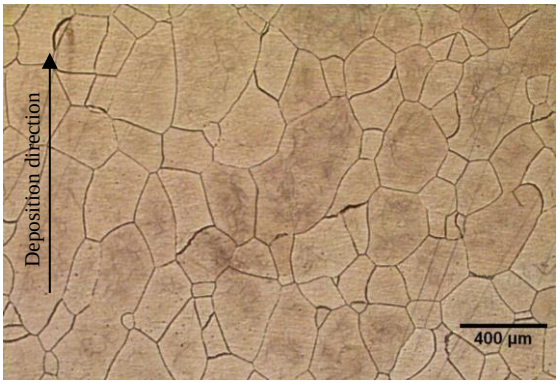

Figure 3-10: Ti-5553 deposited layers adjacent to the interface. The equiaxed grain sizes vary between 250-600µm. The grain sizes increase with the progress of the build.

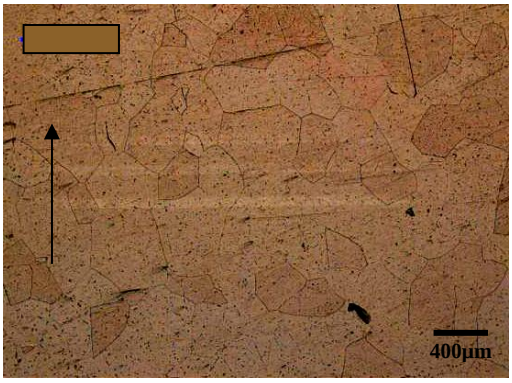

Figure 3-11: Ti-5553 deposited layers at the top layers. The grains have grown considerably and now measure between 400-1000µm.

Figure 3-12: The image taken from the Ti-5553 substrate. The microstructure contains β-matrix with α-phase precipitated within the grains. Large β grains cannot be easily separated in the background.

The substrate (as shown in figure 3-12) contains aged Beta matrix with alpha precipitations. There are 2 categories of the precipitated alpha: Primary & Secondary:

Primary alpha phase has been precipitated during the forging stage. The secondary alpha phase is precipitated during the ageing cycle. The secondary alpha precipitates are extremely fine within the beta matrix. The ageing cycle for this material includes heating the material at temperature 50°C below the beta-transus (β-t) temperature for a period of 8 hours and air cooled to room temperature. This heat treatment cycle has been established by the material specification and the temperature has been specified to be below the beta transus in order to produce as much secondary alpha phase as possible without undesirable growth of beta grains. As illustrated by the figures above, there is a significant difference between the as-deposit structure of the deposited layers and the heat treated substrate.

3.5.3 Mechanical tests on as deposit samples:

Mechanical tests including room temperature tensile testing and micro hardness testing were carried out on the test pieces. Tensile tests were carried out on the samples extracted from the specifically fabricated blocks, but the hardness tests were carried out on the actual test samples.

3.5.3.a – Micro-hardness testing:

Micro-hardness tests were carried out on the substrate and the deposited layers (longitudinally) and transverse to establish the variation of hardness within the deposition and also for comparison purposes between the hardness of the base material away from the heat zone in contrast with the hardness of the heat affected zone.

The results on figure 3-13 show that the hardness has decreased with the progress of the build. Such hardness results variations within the build confirm the increase in the grain size increase as shown previously. This effect has been attributed towards the residual heat from the deposition of each next layer of build.

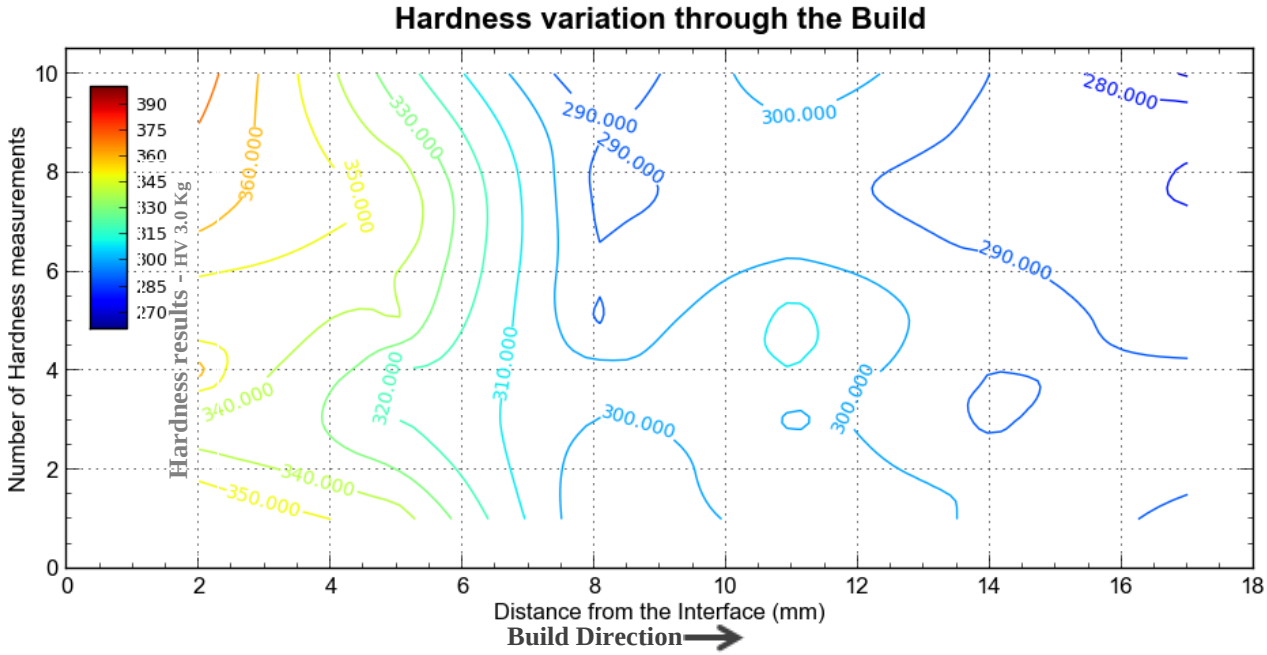

Figure 3-13: Hardness results of the deposition. The readings are taken from the bottom of the build, near to the HAZ towards the top of the build. The results show hardness decrease as the height of the build increases. Vickers hardness test, HV3Kg.

The hardness results on the substrate as plotted in the figure 3-14 show that the hardness has dropped below the HAZ and would increase when measure away from the HAZ.

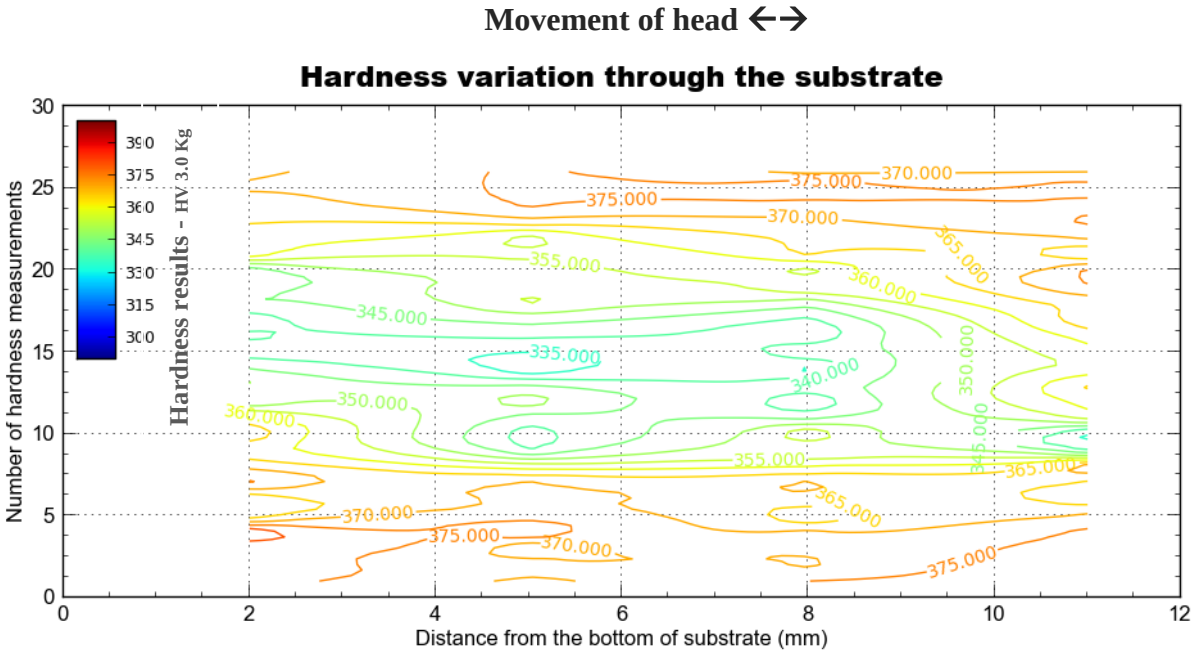

Figure 3-14: Hardness variations from the bottom of the substrate towards the HAZ. Hardness readings taken using HV 3Kg.

3.5.3.b – Tensile testing in as-deposit condition:

Tensile tests were carried out also showed that the minimum mechanical requirements have not been achieved. Table 3-4 show the tensile test results for both longitudinal and transverse test pieces in as-deposit condition.

Sample #	Location	Condition	0.2% P.S. (MPa) achieved	0.2%P.S. Standard	UTS achieved (MPa)	UTS Standard (MPa)
Sample 1	Longitudinal	As deposit	994.9	1170 minimum	1070	1240 minimum
Sample 2	Transverse	As deposit	1035	1170 minimum	1190	1240 minimum

3.6 Microstructural Improvement

As shown above, the as-cast microstructure showed significantly different structure to the base material. No evidence of α-phase precipitation could be seen in the samples. Tensile test results and microstructure analysis of the samples confirm the previous information within the literature. As reported by the reviewed literatures [7, 8, 9], heat treatment cycles are required to facilitate precipitation of α-phase within the β-matrix.

3.6.1 Heat treatment of Deposited Ti-5553 - Ageing cycle

The first heat treatment cycle considered in this study was an ageing cycle. As per Messier-Dowty material specification [25] the recommended ageing cycle for this material is soaking at 600ºC for 8 hours followed by air cool to room temperature. Following this heat treatment cycle, the microstructure showed some precipitated α-phase within aged β-grains as shown in figure 3-15.

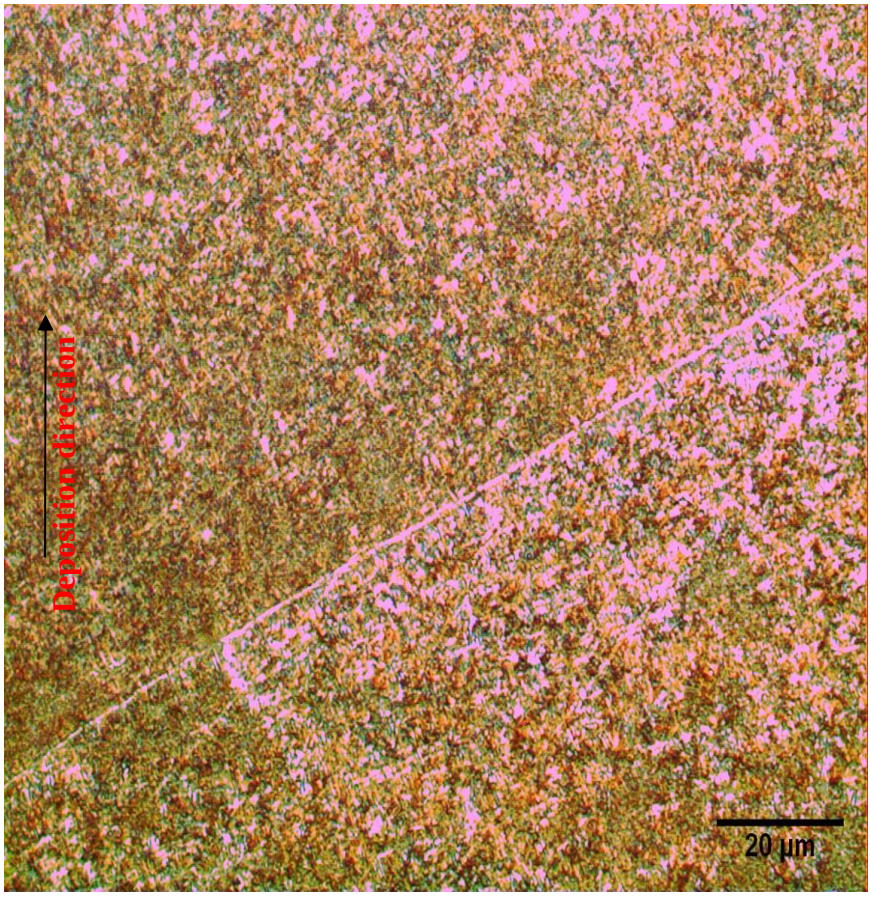

Figure 3-15: Optical micrograph of aged sample. The precipitated alpha is shown in white within the dark beta background. The alpha precipitates are about 1-2 micron in length. The precipitation is not uniform and patchy within the microstructure. In general where, precipitation occurred it has developed Widmanstatten morphology.

The tensile test result for the aged samples showed a marginal improvement in the mechanical properties. The Proof Stress had increased to 1160 MPa, still below the minimum requirement of 1170 MPa, but the ductility has not improved. The test piece failed with almost 4% elongation compared to minimum 6% elongation required on longitudinal test pieces.

3.6.2 Further heat treatments – Solution treatment and Ageing

Based on the metallographic evaluation results and also the mechanical testing results, ageing cycle will not develop adequate α-precipitates. As the result and as

recommended by the published literatures, solution treatment and ageing cycles were investigated.

For this purpose, solution treatment at 50ºC below the β-transus temperature was studied. This temperature was selected to ensure no β transformation happens within the substrate. Such transformations would greatly affect the properties of substrate. Slow cooling is required for the alpha phase to precipitate from the beta matrix. Ageing temperatures of 500°C, 550°C & 600°C were selected and the test pieces were aged for 1 hour at temperature. The test pieces were then subject to tensile testing to select the condition with the most desirable properties for further evaluation. The result of mechanical testing showed that ageing cycle at 600°C had produced the nearest mechanical properties to those of the material specification. The mechanical test results for the sample solution treated at 900°C and aged at 600°C are summarised in table 3-5.

Sample #	Condition	0.2% P.S. (MPa) achieved	0.2%P.S. Standard	UTS achieved (MPa)	UTS Standard (MPa)
Sample 8	Solution Treated @ 900°C& aged @ 600°C	1163 MPa	1170 minimum	1256 MPa	1240 minimum
Samples 9 (Repeated)	Solution Treated @ 900°C& aged @ 600°C	1180 MPa	1170 minimum	1266 MPa	1240 minimum

Table 3-5: Mechanical test results of the solution treated and aged samples. The process was repeated to ensure the repeatability of the results.

Figure 3-16 shows the micro-section of the Solution treat at 900°C and Aged at 600°C sample after polishing and prior to etch. The micro-section appears to be plain without any precipitates in contrast to the micro-section from the substrate as shown in figure 3-17. Considering the fact that the substrate has been subject to a number of Solution treatment and Ageing cycles, the potential growth of the precipitates is expected.

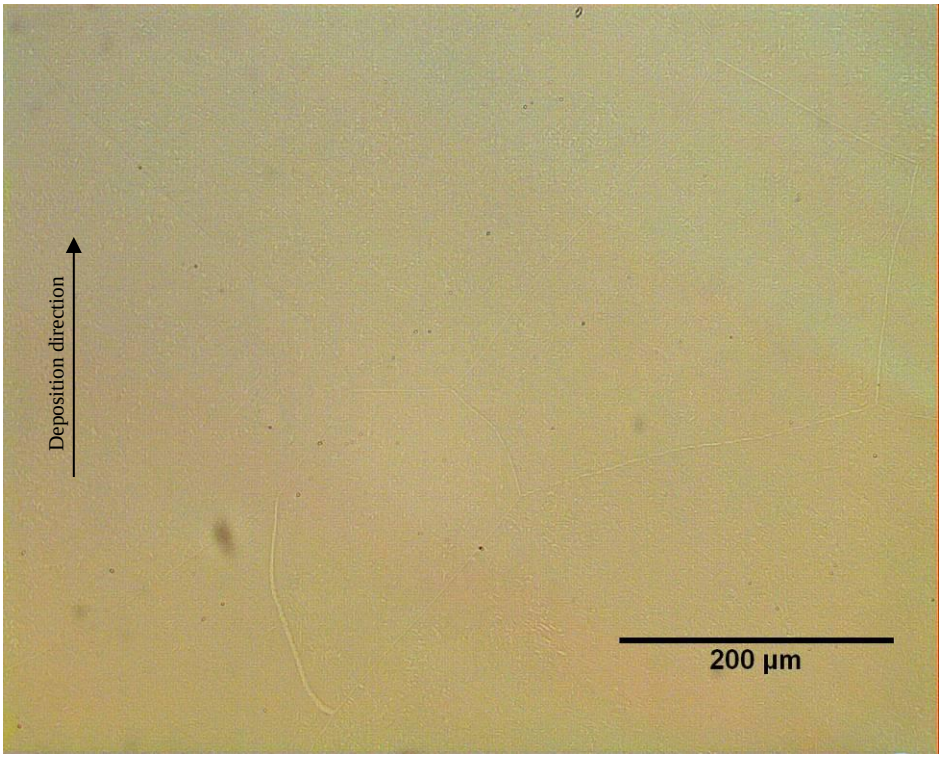

Figure 3-16: The micro-section from the deposition shows plain β – matrix with no α-precipitation.

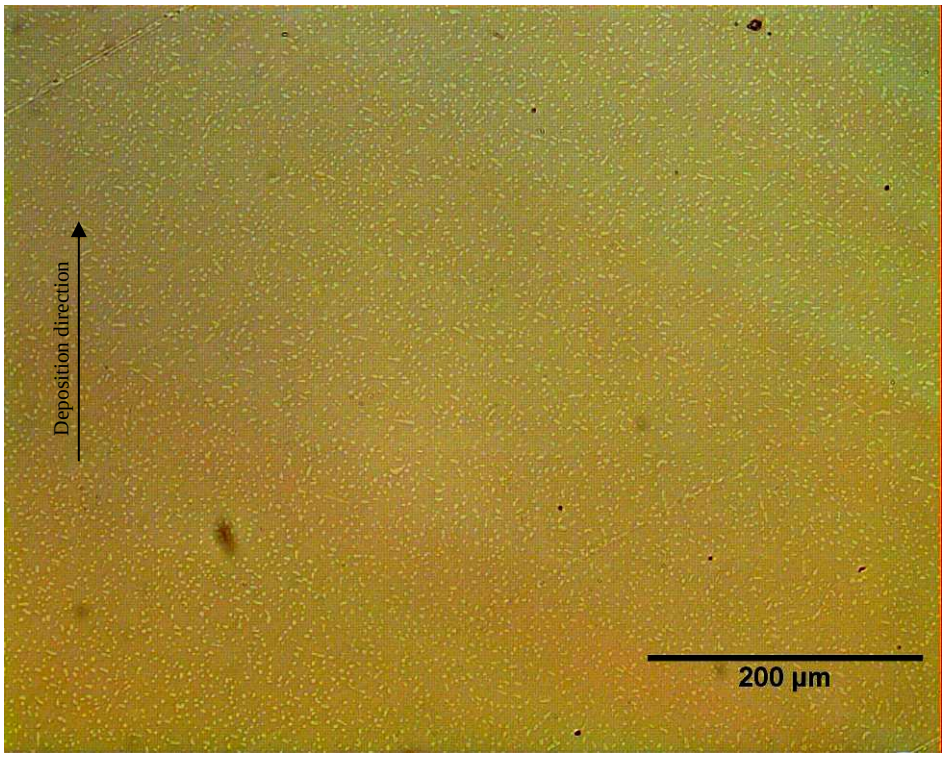

Figure 3-17: In contrast with the deposition layers, the micro-section from the substrate already shows signs of precipitation. This will be confirmed when the samples has been etched and grains and precipitates are revealed.

The etched micro-section of both the substrate (figure 3-18) and deposition (figure 3-19) samples show that significant precipitation of α-phase has occurred within the aged β-matrix.

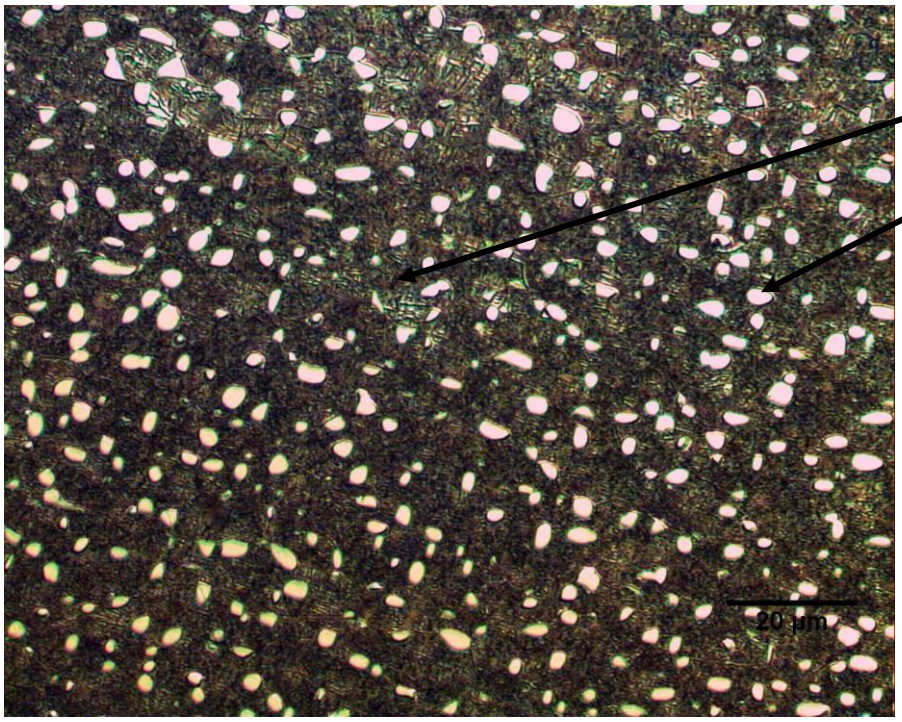

Figure 3-18: Optical micrograph of base material. Primary alpha in clusters precipitated at the forging stage with extremely fine secondary alpha within Beta background precipitated during the ageing stage. Etched in Krolls.

The α-precipitates in substrate shown in white are in 2 main categories: Primary α that have deposited during the first heat treatment cycle at forging stage and Secondary α phase precipitated during the final heat treatment. However due to the repeat of the heat treatment it is anticipated that the primary α precipitates have increased in size and also developed more spherical shape.

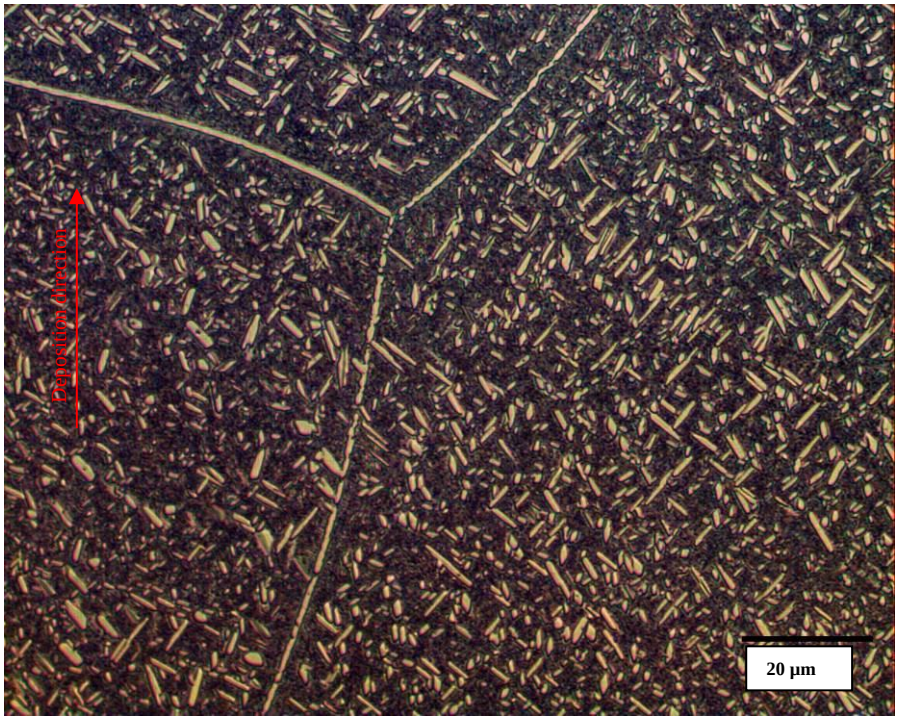

Figure 3-19: Optical micrograph of deposit at higher magnification it can be seen better that needle type alpha precipitations form Widmanstatten morphology. The growth pattern shows dendritic growth on preferred crystallographic directions. Etched

Deposition sample microstructure shows needle shape α-phase precipitation spread within the aged β matrix. The α-precipitates measure between 3-6µm in size. Precipitation also has occurred along the grain boundaries, which as described previously, is an undesirable phenomenon and would create weakness within the structure as the result of the brittleness of α-phase.

3.6.3 Volume fraction analysis of α-phase within β-matrix

Using the image analysis software as described in section 2, volume fraction analysis was carried out to establish the percentage on α/β phases. The image analysis results are shown in figure 3-20 for substrate and figure 3-21 for deposition and the results shown in table 3-5.

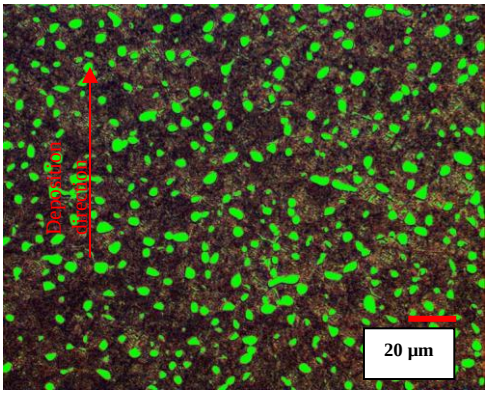

Figure 3-20: Optical micrograph of base material. Threshold was set to separate alpha phase from the beta matrix. Alpha precipitates are shown in green.

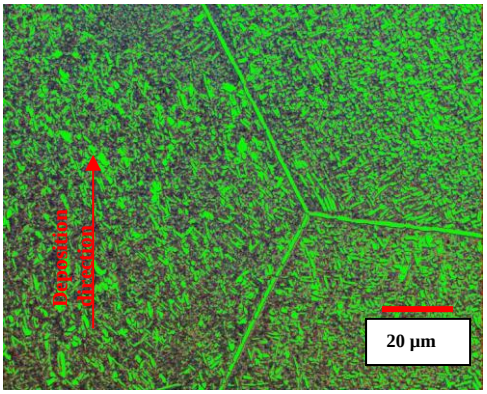

Figure 3-21: Optical micrograph of deposit Thresholds were set to segregate alpha precipitates in needle shape from the beta matrix.

The results of the volume fraction analysis as shown graphically and quantified in table 3-6 suggest that in case of the deposit, the volume of precipitated alpha is almost twice the volume of primary and secondary precipitated alpha in the base metal. This suggests that further work can be carried out to optimise the heat treatment cycles so adequate alpha can be precipitated. Such optimisation can potentially reduce the heat treatment cycle times.

Sample tested	Measured Area	Area Fraction
Substrate	1597.05µm²	10.8 %
Deposition	476.44 µm²	23.5 %

Table 3-6: α-phase area fraction analysis results for Substrate and Deposition.

3.7 Discussion:

The study suggests that the successful DLF depends on 2 main categories of variables: Processing parameters and Metallurgical aspect of the substrate and deposition.

3.7.1 Processing Parameters

The characterisation results of the samples processed with various processing parameters proved that in order to achieve the theoretical build height, Scanning rate, Powder feed rate and the Laser Power must be optimised. Reduction in the scanning speed would increase the build rate and would result in excessive usage of the powder. In opposite, increase in the scanning speed, the previous layer is exposed to the laser power for a shorter time and the overall build rate will be reduced. Since the "Z" parameter is constant, the distance between the laser focal point and the last build layer will increase causing the focal spot to be further away from the build. Once the laser focal point has moved away from the build, the laser will no longer melt the powder and the powder will free flow.

The powder feed rate would also affect the quality of the deposition. High powder feed rates, apart from an unnecessary increase in the powder consumption; will cause the powder to flow back into the nozzle and the laser head causing defects to be formed within the nozzle, as it was seen during the deposition of samples in this project. Lower feed rates on the other hand will result in reduction in deposition rate.

Laser power also affects the deposition results. Inadequate laser power would not melt the substrate so the deposition will not adhere to the surface. Higher laser power would result in higher degree of superheat in the molten metal causing slower cooling rates. However the significance of the laser power effect is on the morphology of the microstructure. Analysis results as reported by J. Liang in his PhD thesis [37] proved that increase in laser power would result in the shift of the morphology from the columnar grains towards equiaxed morphology. However the morphology of the samples in the present study appeared to be equiaxed.

Optimum processing parameters would ensure defect free deposition to be produced as required. However it must be noted that the optimisation must be

carried out for each application and processing parameters from one application can not necessarily be transferred to another application.

3.7.2 Metallurgical aspect

Metallographic studies on the samples showed the microstructure of the as-deposited samples of Ti-5553 to be of β nature with no precipitated α phase. The micrographs of the various build heights showed that grains size increase as the build progresses.

The interface between the substrate and the deposition is clearly defined by the HAZ. Micro-sections proved that grains sizes immediately after the interface are significantly smaller size (200-600µm) when compared to the grain sizes in further distance from the interface (400-1000µm). These results also repeat the conclusion taken by *F.Wang & et al.* [29] as discussed earlier in section 1.4.1.

Micro-section of the interface and the deposition layers did not contain any porosity, although other studies [36] have reported various levels of porosity within the deposition. The study suggested the lower laser powers would result in higher volume of porosity, although the study was carried out on Ti-6Al-4V and not Ti-5553. The powder was not also reported to be PREP® so it may include inherent porosity, which it was shown earlier in this report that PREP® powder does not include inherent pores.

Tensile results of as-deposit samples suggest the mechanical properties of the deposition in this condition to be extremely low. This is also confirmed by the hardness test readings.

The ageing cycle following the deposition showed some improvement and the microscopic observations showed a limited volume of α-phase precipitated within the β-matrix. Tensile properties were also improved but still significantly below the requirements for Ti-5553 material.

Microscopic evaluations showed that Solution treatment and ageing cycle would significantly increase the volume fraction of the α-phase within the β-matrix. The solution treatment in this study was carried out below the β-transus temperature for the substrate in order to ensure the as-forged condition of the substrate is not affected by this heat treatment cycle.

The volume fraction of α-phase in deposition appeared to be higher than the substrate. This can be attributed to the controlled heat treatment cycle and the forging process for manufacturing the substrate.

Micro-section analysis also showed α-precipitates precipitated along the β grain boundaries. This is particularly undesirable due to the ductile nature of the α-phase that would reduce the strength of the material.

The final results were repeatable and were reproduced. The tensile test results showed significant improvement in the mechanical properties of the deposition. The results showed that solution treat and aged samples achieve the minimum U.T.S requirements for Ti-5553, although the proof strength has not successfully reached the minimum requirements. It must be considered that mechanical properties referenced in this report are of those which have been produced by forging process and it is expected to be significantly greater than material produced through casting processes. In comparison, other studies [19] on DLF of Ti-6Al-4V have been reported to reach the material specification limits however due to the limited study on DLF on Ti-5553, the UTS of the solution treat and aged samples as reported in this report exceed the values published by J.C.Fanning *et al.* in his study of DLF of Ti-5553.

3.7.3 Process limitations:

Inherent Process Limitations: One of the major limitations of this technology is extreme difficulty of the systems to be mobile. In cases where the DLF technique

ought to be used in-situ i.e. in case of ad-hoc repairs, the system is non-flexible and cannot be moved easily.

Other inherent limitation is the absolute need of protective atmosphere during the deposition. Experiments proved although protective carrier gas flows through the nozzles, it does not provide adequate protection of the melting pool. As a result special protection chambers have to be set up and the oxygen level must be reduced below 500 PPM to avoid oxidisation during deposition.

4 Conclusion

4.1 Study results

Based on the present study, the following conclusions can be drawn:

- Direct Laser Fabrication process was trialled and modified to adopt Titanium Ti-5553 powder for aircrafts landing gears. The process used the TRUMPF VFA 600 CO2 laser deposition system at the University of Birmingham using PREP Ti-5553 powder.

- The result utilised 3 processing parameters: Scanning Speed, Laser power and Powder feed rate. Microstructures analysis showed that the grain structure is equiaxed as the result of pulsed laser.

- The process optimisation results showed that using PREP ® powder and selecting correct processing parameters will produce microstructures free from porosity. However the desirable beta matrix with precipitated alpha cannot be achieved without some form of heat treatment.

- The heat treatment cycle must include solution treatment followed by precipitation stage. The single precipitation stage would not produce the desirable microstructure and the mechanical properties required.

- Tensile test results showed that mechanical properties are uniform and consistent along the length of the deposition; however these properties vary through the height of the deposition. Higher layers of deposition show slightly reduced mechanical properties. This reduction in the properties can be attributed to the increase in beta grain sizes.

4.2 Limitations:

The limitation during this study can be separated into 2 categories: a) Processing and b) Metallurgical studies.

a) This study was carried out using Ti-5553 available at the time at the University of Birmingham. One limitation during the study availability of new Ti-5553 proved to be of a problem. This was mainly due to the fact that Ti-5553 billets are not readily available to powder manufacturers and therefore long lead times and also high manufacturing costs are associated with the production of the powder. This could have an impact on the study if the existing volume of powder was insufficient for completion of the study.

Other processing limitation during this study was the actual number of variables or processing parameters studied. For each variable of Laser Power, Scanning speed and Flow rate the study was focused on the 3 levels of low, medium and high ensuring that characteristics such as frequency and pulsing method as well as other processing parameters such as "Z" height were unchanged.

The powder used during the process was PREP® powder which as described in this study, contains significantly less inherent effects. Due to the unavailability and the long manufacturing lead time of the Gas atomised powder, this type of powder was not used during the study.

The number of samples produced for each successful combination of processing parameters to prove the repeatability of the process were limited.

Also it must be noted that the dimensions of the samples were kept constant at 20mmX20mm X20mm. It has not been studied if longer and/or wider builds could be successfully produced using the same parameters.

b) The desired microstructures could only be achieved by heat treatment of deposited structure, but the heat treatment cycles could not be applied in-situ using the laser system.

4.3 Future work

The research can be continued in future in a path to achieve the following objectives:

- Effects of powder type on the microstructure: Prep® powder was used during this project which showed no porosity within the build. However it is expected the level of porosity would increase using gas atomised powders, as the result of inherent gas within the particles. Further tests and analysis are required in order to establish the level and effect of porosity on the mechanical properties.

- It is not clear that the optimised processing parameters are independent of the dimensions of the deposition. Future work is suggested in order to establish if the same processing parameters would create the same results at larger dimensions or complex geometries.

- Further work is also recommended in developing heat treatment cycles during deposition process. This can be particularly important when industrialisation of the DLF process is considered. To the knowledge of the author, further Hipping processes are currently being researched for DLF's parts that could include heat treatment cycles; however the need for separate heat treatment process after the deposition can potentially limit the benefits of this technology for in-situ applications.

Appendix A - Powder Analysis Results

Date	24/04/2012 16:11	**µm**	**%**	**% <**	**Size**
		17.18	0.00057	10	64
File name:	ti-5553_01_00.$ls	18.86	0.011	25	81.8
File ID:	ti-5553	20.7	0.05	50	99.6
Sample ID:	ti-5553	22.73	0.11	75	117
Operator:	jw	24.95	0.2	90	131
Bar code:		27.39	0.3		
Comment 1:		30.07	0.42	**Size**	**% <**
Comment 2:		33.01	0.55	1	0
		36.24	0.7	10	0
From	0.375	39.78	0.86	100	50.6
To	2000	43.67	1.04	1000	100
Volume	100	47.94	1.29	**% >**	**Size**
Mean:	98.17	52.62	1.7	10	131
Median:	99.59	57.77	2.43	25	117
D(3,2):	89.03	63.41	3.7	50	99.6
Mean/Median ratio:	0.986	69.61	5.64	75	81.8
Mode:	105.9	76.42	8.28	90	64
S.D.:	25.86	83.89	11.2		
Variance:	668.7	92.09	13.8	**Size**	**% >**
C.V.:	26.34	101.1	15.1	1	100
Skewness:	-0.328	111	14.2	10	100
Kurtosis:	-0.102	121.8	11	100	49.4
d10:	63.97	133.7	5.9	1000	0
d50:	99.59	146.8	1.44		
d90:	130.9	161.2	0.076		
Specific Surf. Area:	673.9				

Note: Due to the nature of Ti-5553 powder, the actual result may be different than shown here fast settlement of Ti-5553 powder suspended in water did not provide adequate time for the laser particles scanner.

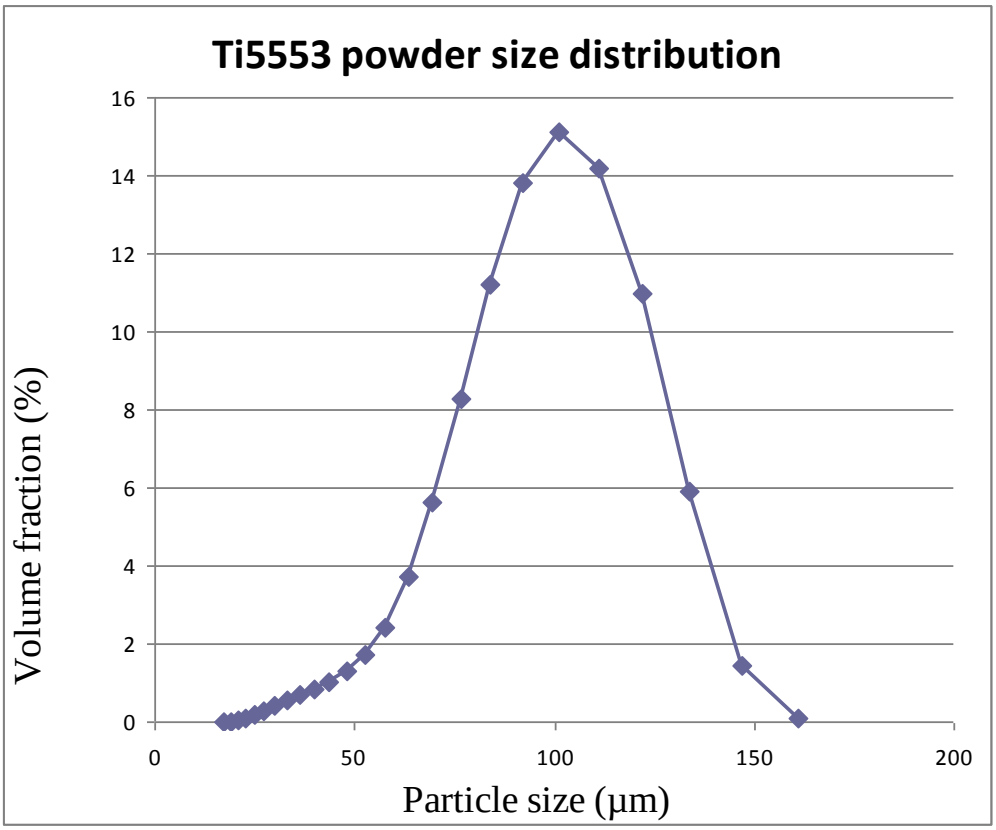
Ti5553 powder size distribution
Volume fraction (%)
16
14
12
10
8
6
4
2
0
0
50
100
150
200
Particle size (μm)

Appendix B - Model design

Boeing B787 Truck Beam has been designed and manufactured by Messier-Dowty Ltd Gloucester. The design utilises a Model Based definition that has been extracted and translated into Catia® model that can be used by the DLF machine.

The stress design of the truck beam requires the entire part to be manufactured through forging process. The forged part includes all the lugs as required by the original design. As mentioned earlier the aim of this study is to establish the possibility of producing those lugs through Laser Deposition technology on the forged cylinder. The cost analysis (details available at Messier-Dowty Ltd, not published due to data confidentiality) carried out at Messier-Dowty had shown the cost of forging complete detailed part is significantly higher than the forging of the main cylinder without the Lugs.

It must also be noted that the samples in this research were produced on flat surfaces. The actual application of this technology on the landing gears would require deposition on curved surface. The deposition model as shown below has been developed to produce the lug as shown in pictures B2 and B3.

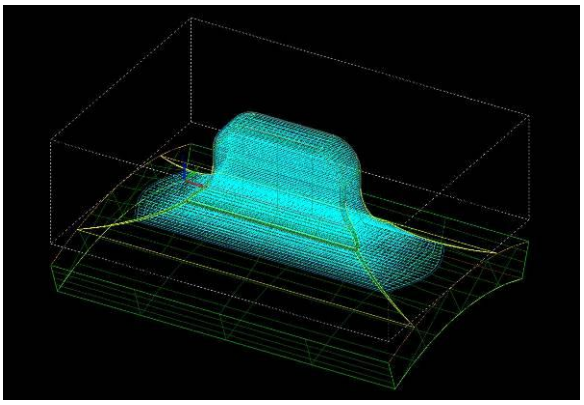

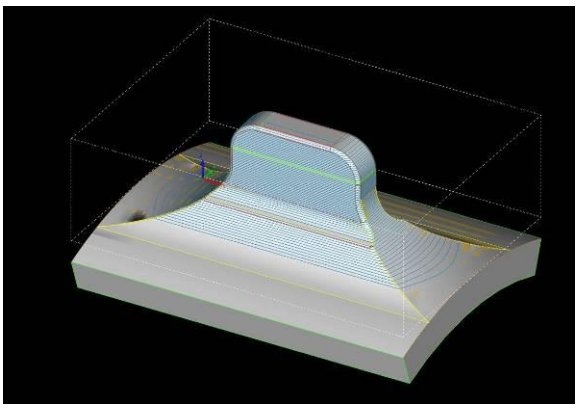

Figures B1-B4: pictures above show the Catia ® model used for the deposition of the lug. Although the model showed deposition on curved surface, the actual deposition was carried out on flat substrate as shown below in figures B3 & B4.

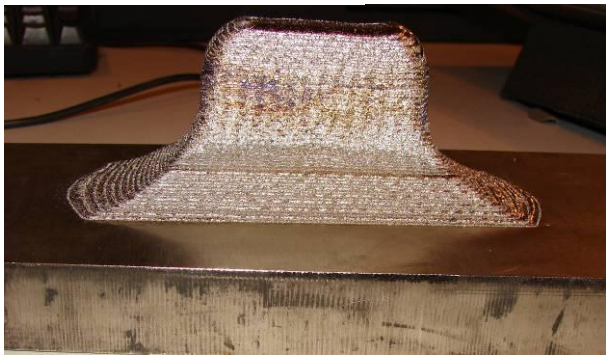

Appendix C - Tensile test results

Wednesday, June 20, 2012 18:46:09

Report Number	RM 35929	
Test Piece Ident	T/P No1	
Part No	Ti 5553	
Specification	MTL-3103 Issue 2	
Special requirements	STA Transverse	
Specification Id #3	SPEC. CHECKED	
Order No	FAO Arash Hatefi	
Date	20/06/2012	
Time	18:40:15	
Geometry Specification Id	Subsiduary 1/4 BSF	
Machine Operator	AW	
Cross-Sectional Area	12.254	mm²
Diameter	3.95	mm
Specimen Geometry	Solid Circular Bar	
Specimen Gauge Length	16.59	mm
Parallel Length	28	mm
Extensometer Gauge Length	25	mm
Maximum Load	13.113	kN
Ultimate Tensile Strength	**F 1070**	**MPa**
Fracture Strength	250.66	MPa
Young's Modulus	103.66	GPa
Rp1(0.2%)	**F 994.97**	**MPa**
Temperature	Ambient	
% Elongation	7.3538	
% Reduction in Area	36	
Comment	FAO Arash Hatefi	PE8780
Test Type	Tensile	
Test Standard	ASTM E8	

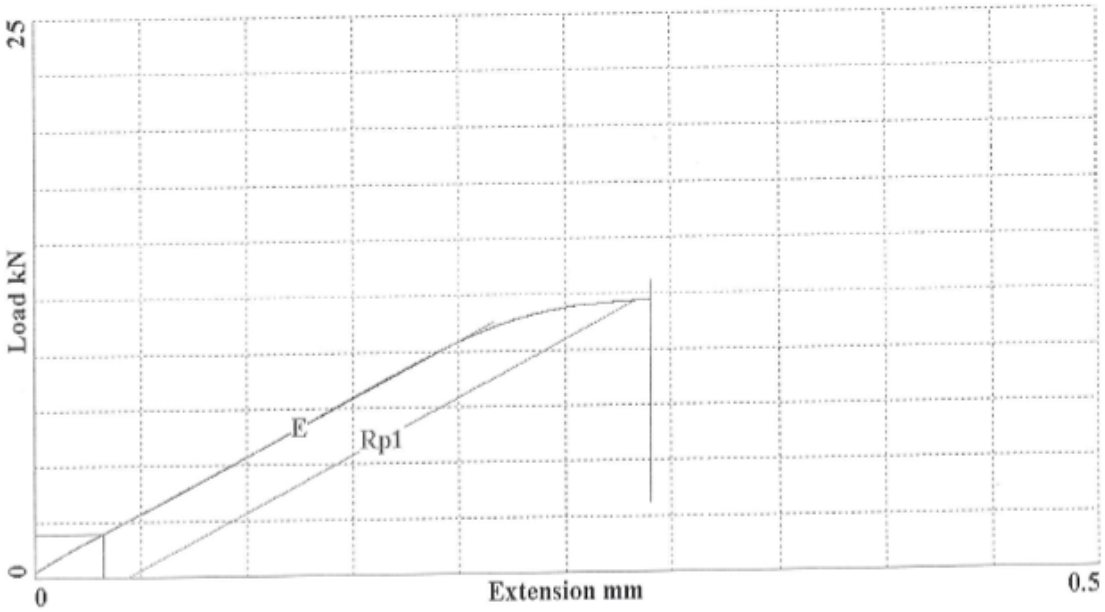

Report Number.....:	RM 35930		
Test Piece Ident.....:	T/P No2		
Part No.....:	Ti 5553		
Specification.....:	MTL-3103 Issue 2		
Special requirements.....:	STA Transverse		
Specification Id #3.....:	SPEC. CHECKED		
Order No.....:	FAO Arash Hatefi		
Date.....:	20/06/2012		
Time.....:	18:54:47		
Geometry Specification Id.....:	Subsiduary 1/4 BSF		
Machine Operator.....:	AW		
Cross-Sectional Area.....:	12.441	mm²	
Diameter.....:	3.98	mm	
Specimen Geometry.....:	Solid Circular Bar		
Specimen Gauge Length.....:	16.31	mm	
Parallel Length.....:	28	mm	
Extensometer Gauge Length.....:	25	mm	
Maximum Load.....:	14.529	kN	
Ultimate Tensile Strength.....:	**F 1167.8**	**MPa**	
Fracture Strength.....:	262.17	MPa	
Young's Modulus.....:	110.17	GPa	
Rp1(0.2%).....:	**F 1102.9**	**MPa**	
Temperature.....:	Ambient		
% Elongation.....:	**F 1.6554**		
% Reduction in Area.....:	4.4715		
Comment.....:	FAO Arash Hatefi		PE8780
Test Type.....:	Tensile		
Test Standard.....:	ASTM E8		

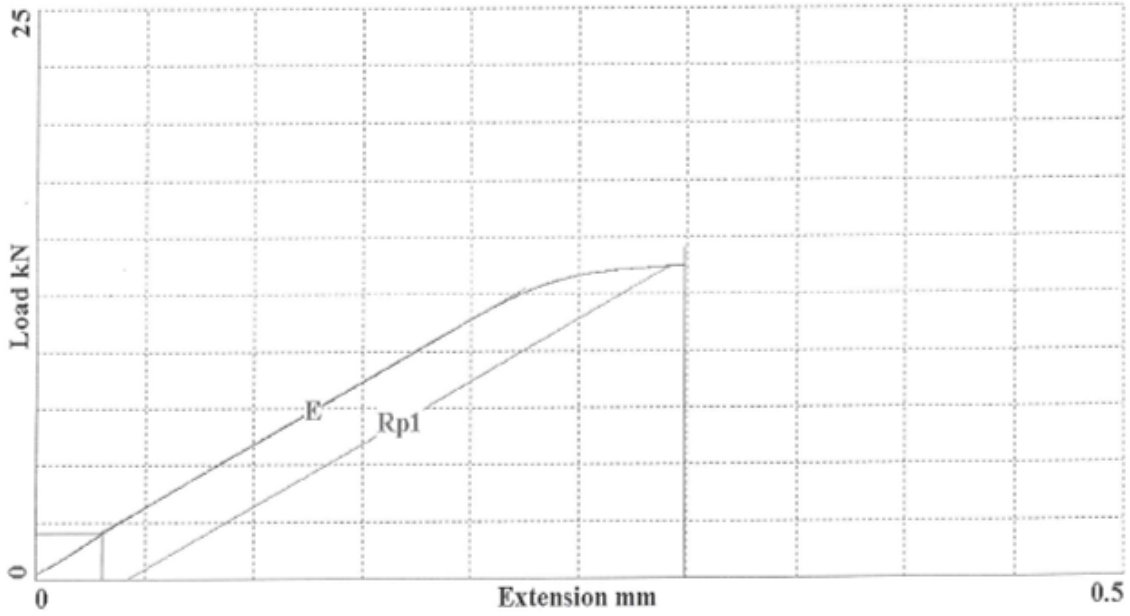

Thursday, June 21, 2012 14:20:00

Report Number.....:	RM 35938	
Test Piece Ident.....:	T/P No3	
Part No.....:	Ti 5553	
Specification.....:	MTL-3103 Issue 2	
Special requirements.....:	STA Transverse	
Specification Id #3.....:	SPEC. CHECKED	
Order No.....:	FAO Arash Hatefi	
Date.....:	21/06/2012	
Time.....:	14:15:11	
Geometry Specification Id.....:	Subsiduary 1/4 BSF	
Machine Operator.....:	RH	
Cross-Sectional Area.....:	12.316	mm²
Thickness.....:	4	mm
Width.....:	12.5	mm
Diameter.....:	3.96	mm
Specimen Geometry.....:	Solid Circular Bar	
Specimen Gauge Length.....:	16.42	mm
Parallel Length.....:	28	mm
Extensometer Gauge Length.....:	25	mm
Maximum Load.....:	14.353	kN
Ultimate Tensile Strength.....: F	**1165.4**	**MPa**
Fracture Strength.....:	716.73	MPa
Young's Modulus.....:	111.57	GPa
Rp1(0.2%).....: F	**1111.7**	**MPa**
Temperature.....:	Ambient	
% Elongation.....:	4.933	
% Reduction in Area.....:	4.4938	
Test Type.....:	Tensile	
Test Standard.....:	ASTM E8	

PE119

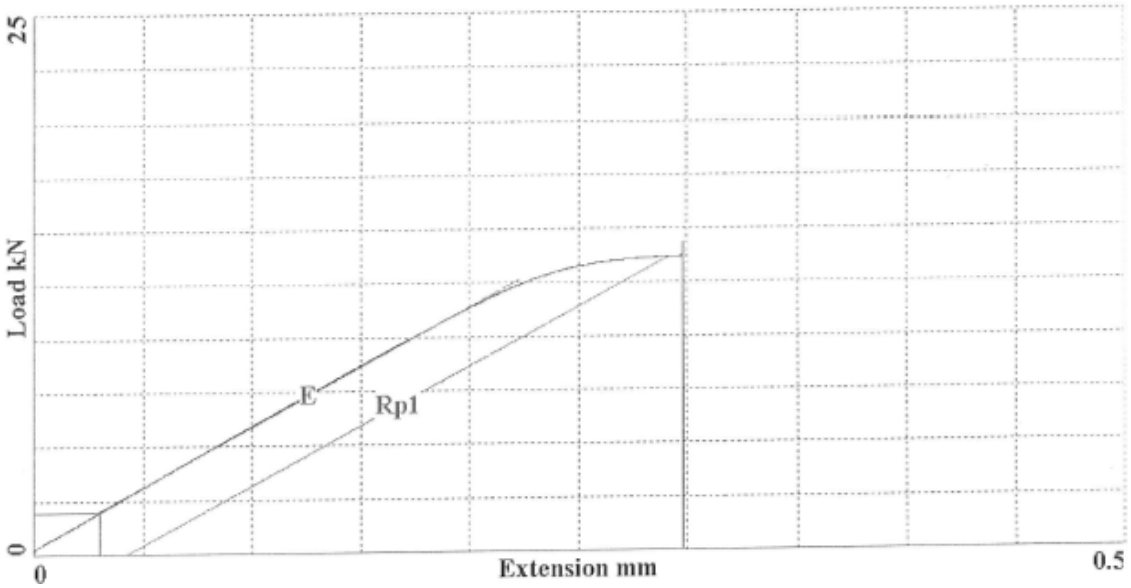

Report Number.....:	RM 35939	
Test Piece Ident.....:	T/P No4	
Part No.....:	Ti 5553	
Specification.....:	MTL-3103 Issue 2	
Special requirements.....:	STA Transverse	
Specification Id #3.....:	SPEC. CHECKED	
Order No.....:	FAO Arash Hatefi	
Date.....:	21/06/2012	
Time.....:	14:22:49	
Geometry Specification Id.....:	Subsiduary 1/4 BSF	
Machine Operator.....:	RH	
Cross-Sectional Area.....:	12.441	mm²
Diameter.....:	3.98	mm
Specimen Geometry.....:	Solid Circular Bar	
Specimen Gauge Length.....:	16.8	mm
Parallel Length.....:	28	mm
Extensometer Gauge Length.....:	25	mm
Maximum Load.....:	7.4742	kN
Ultimate Tensile Strength.....:	**F 600.77**	**MPa**
Fracture Strength.....:	256.68	MPa
Temperature.....:	Ambient	
Comment.....:	t/p failed before proof result	PE119
Test Type.....:	Tensile	
Test Standard.....:	ASTM E8	

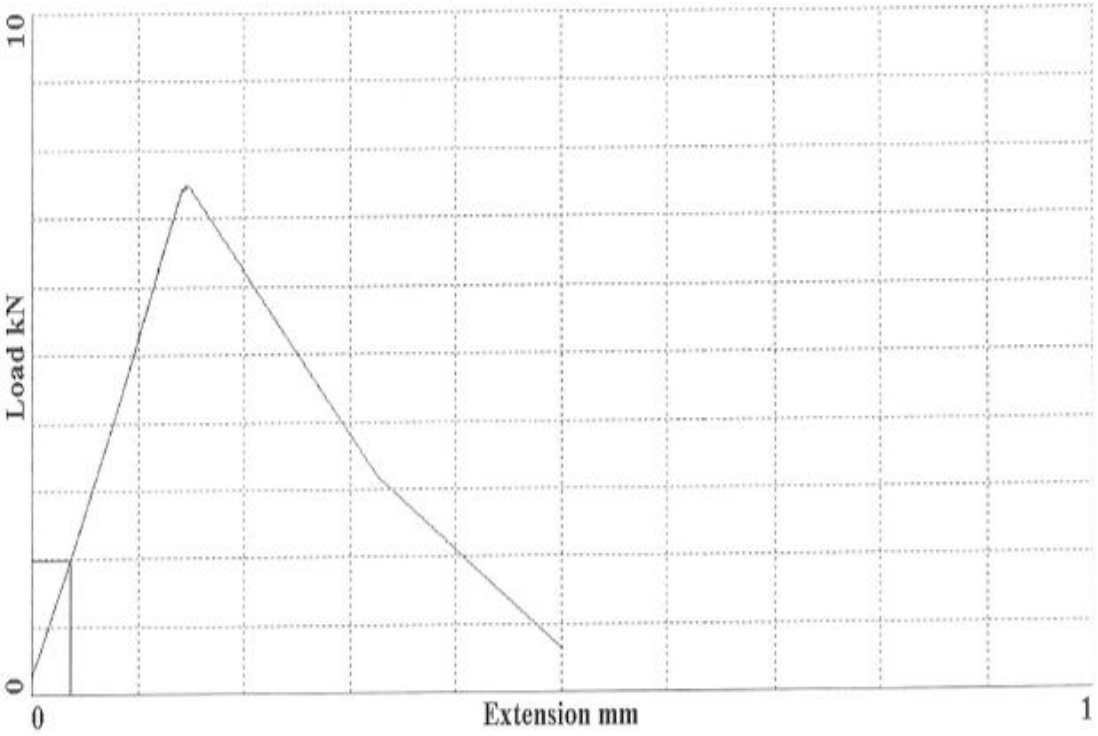

Report Number.....:	RM 35940		
Test Piece Ident.....:	T/P No5		
Part No.....:	Ti 5553		
Specification.....:	MTL-3103 Issue 2		
Special requirements.....:	STA Transverse		
Specification Id #3.....:	SPEC. CHECKED		
Order No.....:	FAO Arash Hatefi		
Date.....:	21/06/2012		
Time.....:	14:31:30		
Geometry Specification Id.....:	Subsiduary 1/4 BSF		
Machine Operator.....:	RH		
Cross-Sectional Area.....:	12.504	mm²	
Diameter.....:	3.99	mm	
Specimen Geometry.....:	Solid Circular Bar		
Specimen Gauge Length.....:	16.82	mm	
Parallel Length.....:	28	mm	
Extensometer Gauge Length.....:	25	mm	
Maximum Load.....:	13.998	kN	
Ultimate Tensile Strength.....:	**F 1119.5**	**MPa**	
Fracture Strength.....:	557.97	MPa	
Young's Modulus.....:	95.468	GPa	
Rp1(0.2%).....:	**F 1035.4**	**MPa**	
Temperature.....:	Ambient		
% Elongation.....:	12.842		
% Reduction in Area.....:	19.945		
Test Type.....:	Tensile		
Test Standard.....:	ASTM E8		

PE119

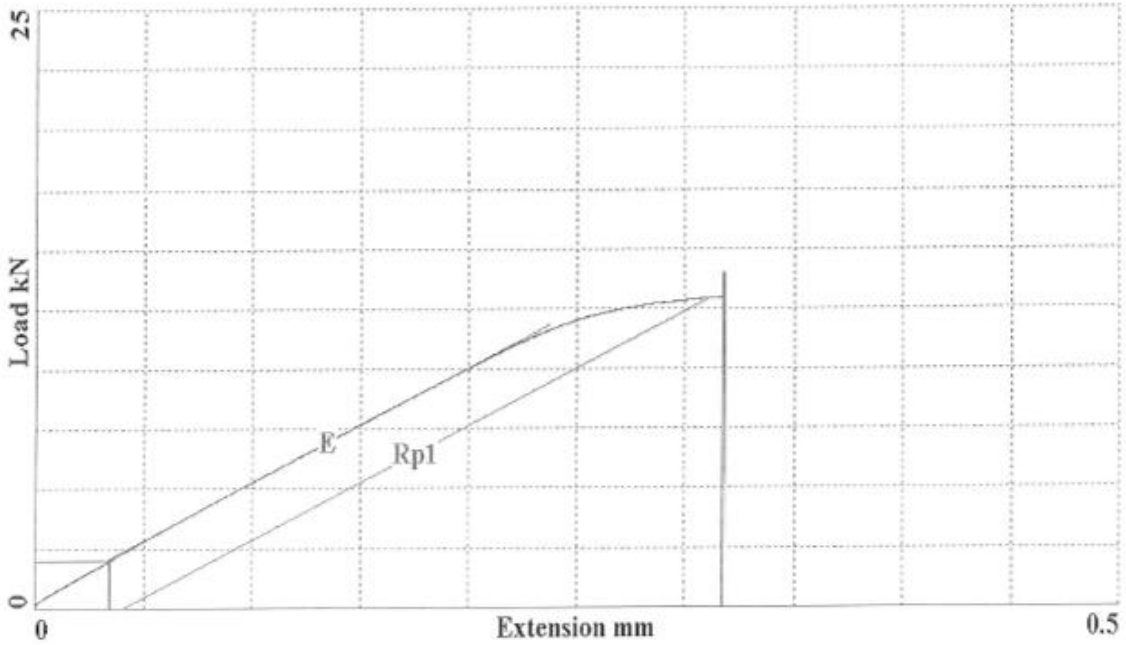

Thursday, June 21, 2012 14:40:20

Report Number.....:	RM 35941	
Test Piece Ident.....:	T/P No6	
Part No.....:	Ti 5553	
Specification.....:	MTL-3103 Issue 2	
Special requirements.....:	STA Transverse	
Specification Id #3.....:	SPEC. CHECKED	
Order No.....:	FAO Arash Hatefi	
Date.....:	21/06/2012	
Time.....:	14:39:58	
Geometry Specification Id.....:	Subsiduary 1/4 BSF	
Machine Operator.....:	RH	
Cross-Sectional Area.....:	12.379	mm²
Diameter.....:	3.97	mm
Specimen Geometry.....:	Solid Circular Bar	
Specimen Gauge Length.....:	16.83	mm
Parallel Length.....:	28	mm
Extensometer Gauge Length.....:	25	mm
Maximum Load.....:	15.092	kN
Ultimate Tensile Strength.....: F	**1219.2**	**MPa**
Fracture Strength.....:	252.72	MPa
Young's Modulus.....:	112.6	GPa
Rp1(0.2%).....: F	**1167.7**	**MPa**
Temperature.....:	Ambient	
% Elongation.....: F	**3.9216**	
% Reduction in Area.....:	2.503	
Comment.....:	failed with extentometer still on	PE119
Test Type.....:	Tensile	
Test Standard.....:	ASTM E8	

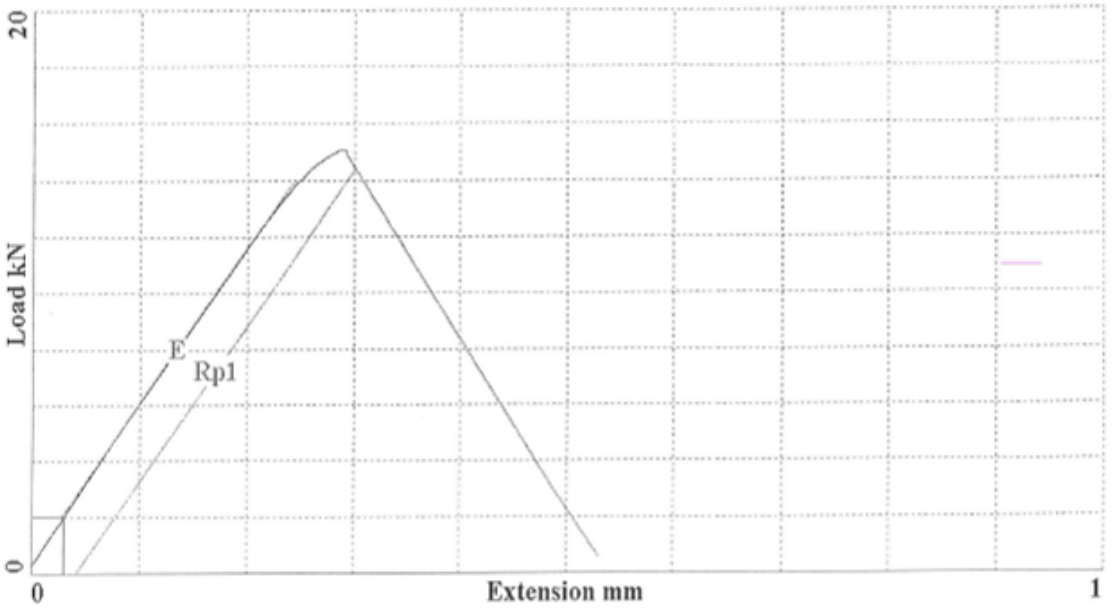

Report Number.....:	RM 35942	
Test Piece Ident.....:	T/P No7	
Part No.....:	Ti 5553	
Specification.....:	MTL-3103 Issue 2	
Special requirements.....:	STA Transverse	
Specification Id #3.....:	SPEC. CHECKED	
Order No.....:	FAO Arash Hatefi	
Date.....:	21/06/2012	
Time.....:	14:49:04	
Geometry Specification Id.....:	Subsiduary 1/4 BSF	
Machine Operator.....:	RH	
Cross-Sectional Area.....:	12.441	mm²
Diameter.....:	3.98	mm
Specimen Geometry.....:	Solid Circular Bar	
Specimen Gauge Length.....:	17.14	mm
Parallel Length.....:	28	mm
Extensometer Gauge Length.....:	25	mm
Maximum Load.....:	15.696	kN
Ultimate Tensile Strength.....:	1261.6	MPa
Fracture Strength.....:	614.23	MPa
Young's Modulus.....:	118.17	GPa
Rp1(0.2%).....:	1259.2	MPa
Temperature.....:	Ambient	
Comment.....:	failed with extentometer still on	PE119
Test Type.....:	Tensile	
Test Standard.....:	ASTM E8	

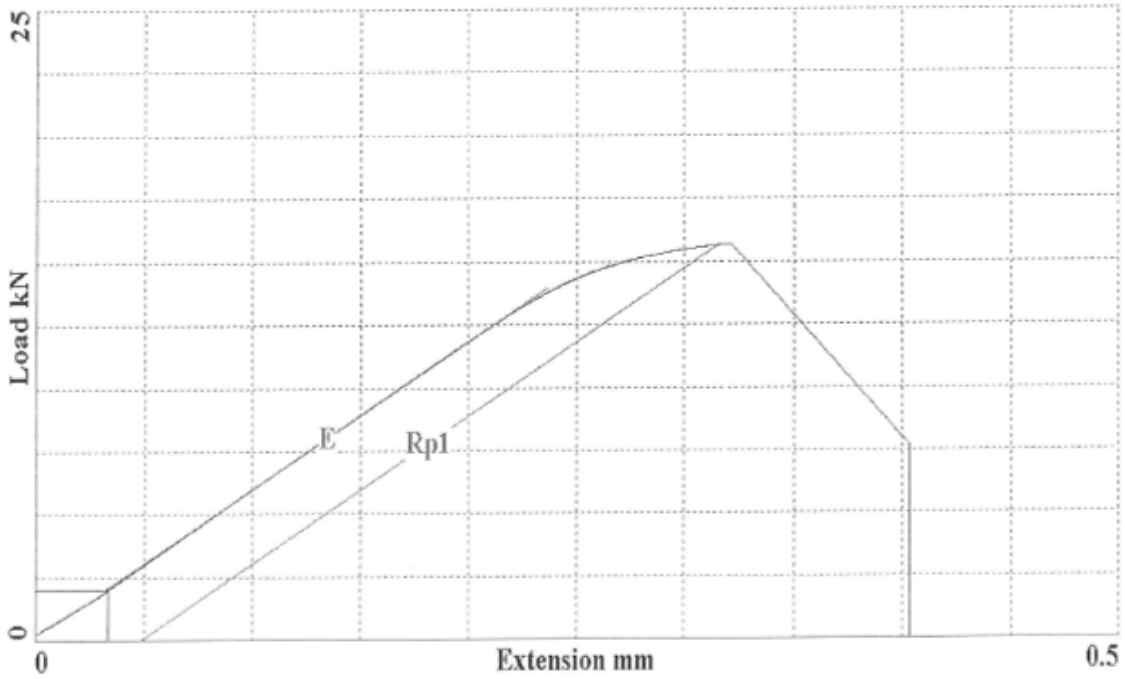

Report Number.....:	RM 35943	
Test Piece Ident.....:	T/P No8	
Part No.....:	Ti 5553	
Specification.....:	MTL-3103 Issue 2	
Special requirements.....:	STA Transverse	
Specification Id #3.....:	SPEC. CHECKED	
Order No.....:	FAO Arash Hatefi	
Date.....:	21/06/2012	
Time.....:	14:58:21	
Geometry Specification Id.....:	Subsiduary 1/4 BSF	
Machine Operator.....:	RH	
Cross-Sectional Area.....:	12.441	mm²
Diameter.....:	3.98	mm
Specimen Geometry.....:	Solid Circular Bar	
Specimen Gauge Length.....:	17.15	mm
Parallel Length.....:	28	mm
Extensometer Gauge Length.....:	25	mm
Maximum Load.....:	15.631	kN
Ultimate Tensile Strength.....:	1256.4	MPa
Fracture Strength.....:	778	MPa
Young's Modulus.....:	109.03	GPa
Rp1(0.2%).....: F	**1163.7**	**MPa**
Temperature.....:	Ambient	
% Elongation.....:	11.603	
% Reduction in Area.....:	12.168	
Test Type.....:	Tensile	
Test Standard.....:	ASTM E8	

PE119

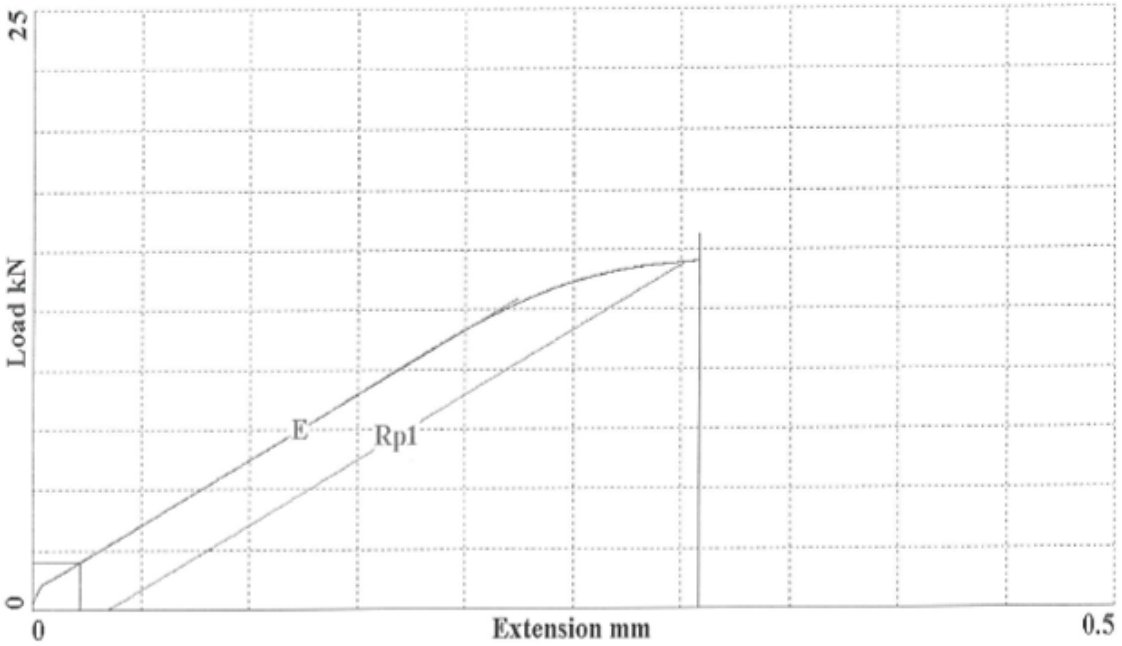

Report Number.....:	RM 35944	
Test Piece Ident.....:	T/P No9	
Part No.....:	Ti 5553	
Specification.....:	MTL-3103 Issue 2	
Special requirements.....:	STA Transverse	
Specification Id #3.....:	SPEC. CHECKED	
Order No.....:	FAO Arash Hatefi	
Date.....:	21/06/2012	
Time.....:	15:06:42	
Geometry Specification Id.....:	Subsiduary 1/4 BSF	
Machine Operator.....:	RH	
Cross-Sectional Area.....:	12.069	mm²
Diameter.....:	3.92	mm
Specimen Geometry.....:	Solid Circular Bar	
Specimen Gauge Length.....:	17.3	mm
Parallel Length.....:	28	mm
Extensometer Gauge Length.....:	25	mm
Maximum Load.....:	15.286	kN
Ultimate Tensile Strength.....:	1266.6	MPa
Fracture Strength.....:	205.56	MPa
Young's Modulus.....:	121.7	GPa
Rp1(0.2%).....:	1180.6	MPa
Temperature.....:	Ambient	
% Elongation.....:	6.4162	
% Reduction in Area.....:	9.9438	
Test Type.....:	Tensile	
Test Standard.....:	ASTM E8	

PE119

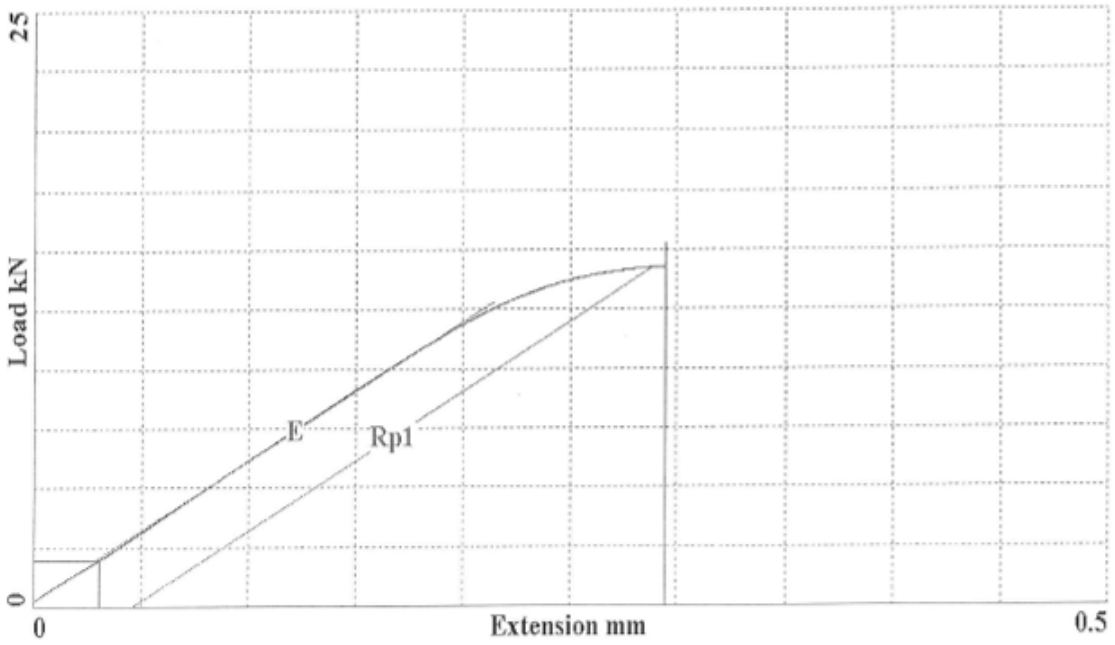

Report Number.....:	RM 35945		
Test Piece Ident.....:	T/P No10		
Part No.....:	Ti 5553		
Specification.....:	MTL-3103 Issue 2		
Special requirements.....:	STA Transverse		
Specification Id #3.....:	SPEC. CHECKED		
Order No.....:	FAO Arash Hatefi		
Date.....:	21/06/2012		
Time.....:	15:15:34		
Geometry Specification Id.....:	Subsiduary 1/4 BSF		
Machine Operator.....:	RH		
Cross-Sectional Area.....:	12.316	mm²	
Diameter.....:	3.96	mm	
Specimen Geometry.....:	Solid Circular Bar		
Specimen Gauge Length.....:	17.34	mm	
Parallel Length.....:	28	mm	
Extensometer Gauge Length.....:	25	mm	
Maximum Load.....:	15.307	kN	
Ultimate Tensile Strength.....:	1242.8	MPa	
Fracture Strength.....:	563.01	MPa	
Young's Modulus.....:	111.73	GPa	
Rp1(0.2%).....: F	**1149.7**	**MPa**	
Temperature.....:	Ambient		
% Elongation.....:	7.3241		
% Reduction in Area.....:	7.9176		
Test Type.....:	Tensile		PE119
Test Standard.....:	ASTM E8		

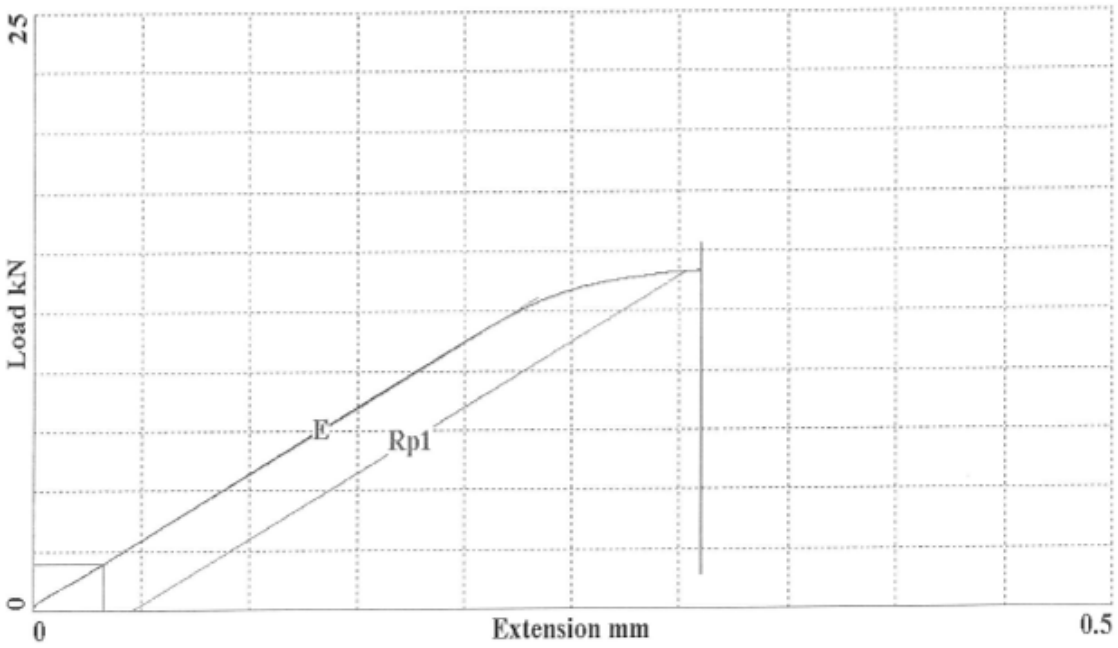

Report Number.....:	RM 35946		
Test Piece Ident.....:	T/P No11		
Part No.....:	Ti 5553		
Specification.....:	MTL-3103 Issue 2		
Special requirements.....:	STA Transverse		
Specification Id #3.....:	SPEC. CHECKED		
Order No.....:	FAO Arash Hatefi		
Date.....:	21/06/2012		
Time.....:	15:22:37		
Geometry Specification Id.....:	Subsiduary 1/4 BSF		
Machine Operator.....:	RH		
Cross-Sectional Area.....:	12.192	mm²	
Diameter.....:	3.94	mm	
Specimen Geometry.....:	Solid Circular Bar		
Specimen Gauge Length.....:	17.25	mm	
Parallel Length.....:	28	mm	
Extensometer Gauge Length.....:	25	mm	
Maximum Load.....:	15.014	kN	
Ultimate Tensile Strength.....:	**F 1231.5**	**MPa**	— 1240
Fracture Strength.....:	474.83	MPa	
Young's Modulus.....:	112.58	GPa	
Rp1(0.2%).....:	**F 1128.4**	**MPa**	
Temperature.....:	Ambient		PE119
% Elongation.....:	9.1014		
% Reduction in Area.....:	11.812		
Test Type.....:	Tensile		
Test Standard.....:	ASTM E8		

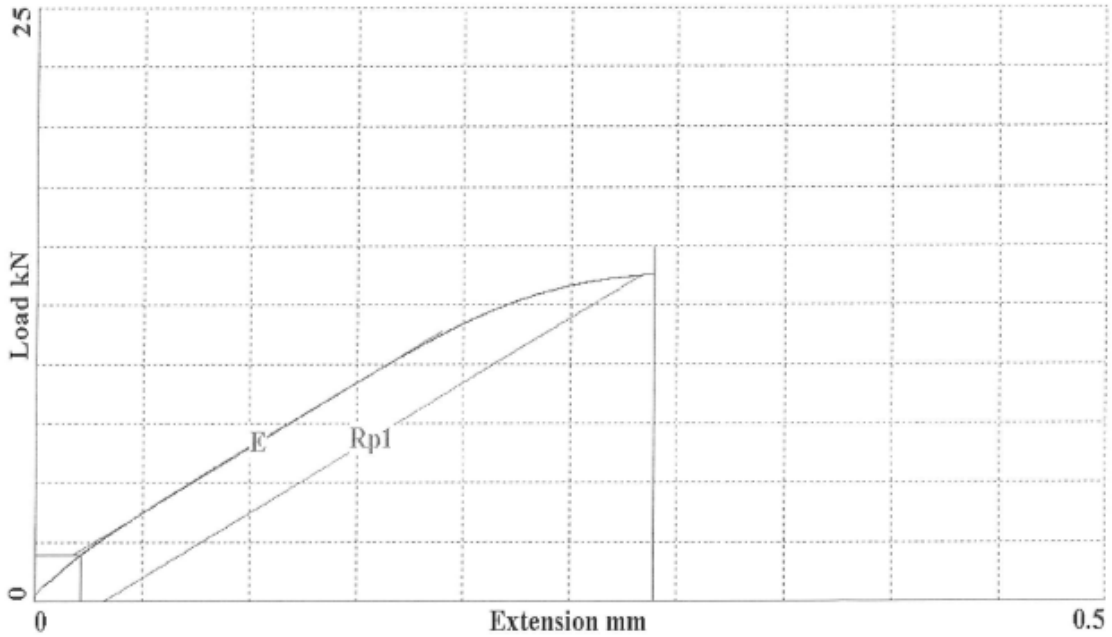

References:

[1] International, A., *Materials Properties Handbook: Titanium Alloys*, ed. R. Boyer, Welsch, G., Collings, E.W. 1994.

[2] E. W. Collings,Materials properties handbook: titanium alloys, Section 2.1

[3] J.N. Fridlyander & D.G. Eskin, Advances in Metallic Alloys, Titanium Alloys, Russian Aircraft and Aerospace applications, Taylor & Francis Group, 2006

[4] Lütjering, G., Williams, J.C., *Titanium*. 2nd ed. 2007: Springer 442.

[5] S. Ankem, C.A. Greene : Materials Science and Engineering A263 (1999) 127–131

[6] *G. Martin et al.*/ Procedia Engineering 10 (2011) 1803–1808

[7] *K.V. SUDHAKAR et al.*, Department of Metallurgical and Materials Engineering, MONTANA Tech of the University of MONTANA, BUTTE, MT 59701, USA

[8] N. Stefansson, I. Weiss, A.J. Hutt, P.G. Allen, P.J., in: P.A. Blenkinsop, W.J. Evans, H.M. Flower (Eds.), Titanium '95, vol. II, The Institute of Materials, London, 1996, pp. 980–987.

[9] *J. Ph. Guibert et al., Les Alliages de Titane Beta, Socie´te´ Franc¸aise de Me´tallurgie et de Mate´riaux,* 1994, pp. 197–204.

[10] R.R. Boyer, R.D. Briggs, J. Mater. Eng. Perform. 14 (2005) 681–685.

[11] N. Clement, A. Lenain, P.J. Journal of Materials Volume 59 (1) (2007) 50–53.

[12] A. Carman *et al.*. / Materials Science and Engineering A 528 (2011) 1686–1693

[13] Ali Dehghan-Manshadi, Rian J. Dippenaar, *Development of α-phase morphologies during low temperature isothermal heat treatment of α Ti–5Al–5Mo–5V–3Cr alloy*, Materials Science and Engineering ,A 528 (2011) 1833–1839

[14] Brain A Welk, Microstructural and Property Relationships in-Titanium Alloy Ti-5553, PhD Research, Ohio State University, 2010

[15] *Nyakana, S.L. et al. , Quick Reference Guide for Titanium Alloys in the 00s.* Journal of Materials Engineering and Performance, 2005. 14(6): p. 799-811.

[16] Beaman, J.J. Marcus, H.L, Bourell, D.L. and Barlow, J.W. (Eds), Proceedings of the solid freefrom fabrication symposium, The University of Texas at Austin, Austin, TX, 1990-94

[17] Messier-Dowty Ltd internal design specifications

[18] G. Lütjering, Materials Science and Engineering A 263 (1999) 117–126.

[19] J.C.Fanning , J. Mat. Eng. Perf. 2005;14(6):788–91.

[20] *S. Nag et. al*. " *ω-Assisted nucleation and growth of α precipitates in the Ti–5Al–5Mo–5V–3Cr–0.5Fe β titanium alloy*", Department of Materials Science and Engineering, University of North Texas, Denton, TX, USA

[21] Duerig TW, Williams JC. *Beta Titanium Alloys in the 80s*: Proceedings of the Symposium. Atlanta, GA: 1984. p. 19–67.

[22] Shevel'kov, V.V., *Structural Conversion in VT22 Titanium Alloy During Aging.* Metal Science and Heat Treatment (Russia), 1992. 34(7-8): p. 534-539.

[23] Orlova, L.M., *Metallographic Study of Solid Solution Decomposition for Titanium Alloy VT22.* Metal Science and Heat Treatment (Russia), 1986. 28(1): p. 73-77.

[24] Messier-Dowty Ltd Material Specification MTL 3103, issue 4.

[25] Messier-Dowty R&T department, internal cost verification in 2011.

[26] Fehmi Erzincahn, Mehmet Ermorat, *Comparison of Direct Metal Laser Fabrication Technologies*, Gebze Institute of Technology, Turkey

[27] Wu, X. (2006) *Net Shape Manufacturing of Aeroengine Components.* In Cost Effective Manufacture via Net-Shape Processing (pp. 5-1 – 5-10). Meeting Proceedings RTO-MP-AVT-139, Paper 5

[28] *W.U.H. Syed et al.* / Applied Surface Science 247 (2005) 268–276

[29] *F. Wang et al., Microstructure study of direct laser fabricated Ti alloys using powder and wire,* Applied Surface Science 253 (2006) 1424–1430

[30] *Yuchang Fu et al., A theoretical model for laser and powder particles interaction during laser cladding*. Journal of Materials Processing Technology, Vol 128, Issues 1-3 (2002) 106-112

[31] *X. Wu et al., Microstructures of laser-deposited Ti–6Al–4V /* Materials and Design 25 (2004) 137–144

[32] *M.N. Ahsan et al., A comparative study of laser direct metal deposition characteristics using gas and plasma-atomized Ti–6Al–4V powders,* Materials Science and Engineering A 528 (2011) 7648– 7657

[33] M.N. Ahsan, C.P. Paul, L.M. Kukreja, A.J. Pinkerton, Journal of Materials Processing Technology 211 (4) (2011) 602–609.

[34] Yunchang Fu, A.Loredo, B.Martin, *A theoretical model for laser and powder particles interaction during laser cladding,* Journal of Materials Processing Technology Vol. 128, Issues 1-3 (2002) 106-112

[35] S.Y. Wen et al. *Modeling of coaxial powder flow for the laser direct deposition process* / International Journal of Heat and Mass Transfer 52 (2009) 5867–5877

[36] Messier-Dowty Ltd Specification, Mechanical testing requirements.

[37] Jing Liang, PhD Thesis, University of Birmingham, 2004

[38] *P.A. Kobryn & et al. The effect of laser power and traverse speed on Microstructure, porosity and build height in laser-deposited Ti-6Al-4V,* Scripta materialia. 43 (2000) 299–305

[39] Proceedings to ICALEO 2009, *Kamran Shah & et al. Parametric study of development of Inconel-steel functionally graded materials by laser direct metal deposition*,

[40] Proceedings to PICALO 2008, *M. Guirad & et al. Process Control on Laser Cladding by Coaxial Vision for Direct Manufacturing of 3D Metallic Structures*